Classification and Parameter Estimation of Asynchronously Received PSK/QAM Modulated Signals in Flat-Fading Channels

William C. Headley

Thesis submitted to the Faculty of the
Virginia Polytechnic Institute and State University
in partial fulfillment of the requirements for the degree of

Master of Science
in
Electrical Engineering

Claudio R. C. M. da Silva, Chair
R. Michael Buehrer
Allen B. MacKenzie

April 30, 2009
Blacksburg, Virginia

Classification and Parameter Estimation of Asynchronously Received PSK/QAM Modulated Signals in Flat-Fading Channels

William C. Headley

ABSTRACT

One of the fundamental hurdles in realizing new spectrum sharing allocation policies is that of reliable spectrum sensing. In this thesis, three research thrusts are presented in order to further research in this critical area. The first of these research thrusts is the development of a novel asynchronous and noncoherent modulation classifier for PSK/QAM modulated signals in flat-fading channels. In developing this classifier, a novel estimator for the unknown channel gain and fractional time delay is developed using a method-of-moments based estimation approach. For the second research thrust of this thesis, the developed method-of-moments based estimator is extended to estimate the signal-to-noise ratio of PSK/QAM modulated signals in flat-fading channels, in which no *a priori* knowledge of the modulation format and channel parameters is assumed. Finally, in the third research thrust, a distributed spectrum sensing approach is proposed in which a network of radios collaboratively detects the presence, as well as the modulation scheme, of a signal through the use of a combination of cyclic spectrum feature-based signal classification and an iterative algorithm for optimal data fusion.

This work is due in large part to the support of the Bradley Fellowship Program at Virginia Tech.

Acknowledgments

There are many people I would like to thank for making this work possible. First, I would like to thank my family and friends for always being a phone call away. I do not know what I would have done without all of you believing in me. Secondly, I would like to thank my advisor, Dr. Claudio da Silva, and the other members of my thesis committee, Dr. Michael Buehrer and Dr. Allen MacKenzie. I especially want to thank Dr. da Silva for always pushing me to be better, and for always being there to help. Thirdly, I want to thank the staff, faculty, and fellow students of the wireless program at Virginia Tech. With their support, they have always made the school a nurturing place to work and to study.

Finally, I want to thank the Bradley Fellowship program for believing in my abilities through their financial support of my graduate education. It is truly with the help of this fellowship that I have been able to continue my education in order to realize my career goals.

Contents

List of Figures

List of Tables

Chapter 1

Introduction

At present, the allocation of spectrum resources for wireless applications is done mainly through the use of fixed and rigid spectrum licenses, in which a licensed user has exclusive rights to its spectrum band [1]. It has been shown recently that this spectrum allocation policy is detrimental to the efficient use of spectrum resources. For instance, [2] and [3] present spectrum occupancy measurements at different geographical locations that demonstrate the severe underutilization of the spectrum under this current regulatory policy. The Federal Communications Commission (FCC) has acknowledged this spectrum underutilization through [4], in which the following statement is made: "Preliminary data and general observations indicate that many portions of the radio spectrum are not in use for significant periods of time."

In order to deal with this spectrum underutilization problem, the FCC recently issued a Notice of Proposed Rule Making (NPRM) in which new methods of spectrum utilization were proposed [5]. In particular, this NPRM describes the potential of spectrum sharing strategies in which secondary cognitive radio users, defined as radios able to intelligently learn and adapt to changes as a function of location/time/frequency [6], efficiently share the spectrum with legacy licensed primary users without causing interference to these users. Based on these ideas presented by the NPRM, a new wireless standard based on the use of cognitive radios is being developed through the IEEE 802.22 Working Group [7]. The goal of this standard is to develop a spectrum sharing environment in the severely underutilized TV band as a means of providing wireless broadband access to rural and

remote geographical areas. It is for these reasons, among others, that a significant research thrust in cognitive radio technologies has developed in recent years. For example, an overview of cognitive radio research at Virginia Tech can be found in [8].

One of the most difficult hurdles in the implementation of cognitive radios in spectrum sharing environments is that of performing reliable spectrum sensing [9]-[12]. Spectrum sensing can be thought of as one, or a combination, of the following (dependent on the *a priori* knowledge of the signals in the environment): signal detection, signal classification (single-carrier/multi-carrier, modulation format, etc.), and signal parameter estimation. Without reliable spectrum sensing, secondary cognitive radio users operating in spectrum sharing environments can potentially cause unintentional interference to other secondary users, or more importantly, to legacy primary licensed users. Spectrum sensing is more difficult in these environments due to the fact that co-existing systems may be uncooperative (especially primary users), and thus no, or little, information may be known about these systems' transmitted signals (such as modulation format, channel gain, carrier phase, time delay, etc.). A recent overview of spectrum sensing research for cognitive radio applications can be found in [13].

In addition to the implications on cognitive radio applications, spectrum sensing also has implications in military applications. For instance, reliable spectrum sensing can allow for more efficient jamming and anti-jamming procedures, as well as an increased ability to intercept enemy communications [14]. It is due in part to these important uses for spectrum sensing that research in this area continues to be of fundamental importance.

Chapters 2 and 3 of this thesis expand upon prior spectrum sensing research, such as [15]-[19], by developing a novel method for the *asynchronous* and *noncoherent* sensing of PSK/QAM modulated signals (termed digital amplitude-phase modulated signals in the following) in flat-fading channels. More specifically, Chapter 2 develops a novel estimator for the unknown channel gain and fractional time delay through the use of a method-of-moments based estimation approach. Using these estimates, a novel classifier for the unknown digital amplitude-phase modulation scheme is proposed based upon a composite hypothesis testing approach known as the quasi-hybrid likelihood ratio test. Chapter 3 of this thesis expands upon the method-of-moments based estimation approach developed in Chapter 2 in order to develop a novel *asynchronous*, *noncoherent*, and *non-data-aided*

signal-to-noise ratio estimator for these signal types.

Chapter 4 of this thesis develops a novel *distributed* approach to *asynchronous* signal detection and modulation classification through the use of a set of cooperative cyclic spectrum feature-based classification radios, a fusion center, and an iterative algorithm for optimal data fusion. More specifically, the set of spectrum sensing radios are assumed to make a local classification decision, determined through the use of the observed signal's cyclic spectrum estimate, that is sent to the fusion center. The fusion center (a spectrum sensing radio itself) then makes the final global decision for the system based upon its own cyclic spectrum estimate, as well as the set of local decisions made by the spectrum sensing radios. In order to determine the local decisions at each radio, as well as the final global decision at the fusion center, person-by-person optimal decision rules are determined through the use of a non-linear Gauss-Seidel iterative algorithm [20].

Chapter 2

Asynchronous Classification of Digital Amplitude-Phase Modulated Signals in Flat-Fading Channels

2.1 Motivation for Work

This chapter concerns the development of an *asynchronous* and *noncoherent* likelihood-based modulation classifier for digital amplitude-phase modulated signals in flat-fading channels. Though much work has been done on developing *synchronous* likelihood-based modulation classifiers in recent years (see [21] for a great listing of such work), to the best of our knowledge the modulation classification of asynchronously received signals in flat-fading channels has not been considered[1]. This apparent lack of research can be attributed to the fact that, for likelihood-based approaches to modulation classification, each of the unknown signal parameters must be handled with no knowledge of the modulation scheme, either by removing the classifier's dependence on the unknowns through the use of their probability density functions (pdf), or through the classifier's use of estimates of the unknowns, each of which is made especially difficult in an asynchronous environment.

[1]For AWGN channels, Beidas and Weber present asynchronous likelihood-based classifiers for MFSK signals in [22] and [23].

2.2 Contribution

This chapter proposes an *asynchronous* and *noncoherent* modulation classifier for digital amplitude-phase modulated signals in flat-fading channels. This classifier is based upon a composite hypothesis testing approach known as the quasi-hybrid likelihood ratio test (qHLRT), in which estimates of the unknown amplitude, phase, and fractional time delay are required. For estimating the unknown amplitude and fractional time delay, a *novel* estimator based upon the method-of-moments is proposed which requires no prior knowledge of the modulation scheme of the received signal. Performance results are presented for the proposed estimator and modulation classifier assuming the use of both rectangular and square root-raised cosine pulse shapes. These performance results show that the proposed asynchronous classification system performs well compared to previously developed synchronous classifiers, given an adequate observation interval.

2.3 Likelihood-based Modulation Classification Techniques

The modulation classification process can be formally defined as: *Given a received signal $r(t)$, determine the modulation scheme used to represent the data from among the c possible modulation schemes $H_1, H_2, \ldots, H_c$.* This is a hypothesis testing problem in which, as the name implies, the correct hypothesis is determined by testing $r(t)$ against each hypothesis H_i, $i = 1, 2, \ldots, c$. In traditional likelihood-based hypothesis testing modulation classification problems, it is assumed that the signal parameters and the probability of each modulation scheme being used, $P(H_i)$, are known. For these problems, a Bayesian approach can be used, which leads to a decision rule that minimizes the probability of classification error [24]. This approach classifies the received signal by finding the maximum among the *a posteriori* probabilities $P(H_i|r(t))$. When each of the possible modulation schemes are equally likely to be used (as will be assumed in the following), an equivalent classifier is the maximum-likelihood classifier, which finds the maximum among $p(r(t)|H_i)$.

When the non-data signal parameters are considered unknown, these traditional testing methods must be extended. This is conventionally known as composite hypothesis testing [24]. For modulation classification applications, there are three main composite hypothesis testing approaches typically considered (differing in how each handle the unknown parameters): the Average Likeli-

hood Ratio Test (ALRT) ([15],[16]), the Generalized Likelihood Ratio Test (GLRT) [17], and the Hybrid Likelihood Ratio Test (HLRT) ([18],[19]). Presented in the following is a brief summary of each of these approaches (for a more detailed discussion on these approaches, refer to [21]).

For the ALRT, the set of unknown signal parameters, $\mathbf{u}$, is considered to be random with known conditional pdf $p(\mathbf{u}|H_i)$. Given this conditional pdf, the dependence on the unknowns is removed by "averaging out" the set of parameters through

$$p(r(t)|H_i) = \int p(r(t)|\mathbf{u}, H_i)p(\mathbf{u}|H_i)d\mathbf{u}, \tag{2.1}$$

where $p(r(t)|\mathbf{u}, H_i)$ is the pdf of $r(t)$ conditioned on the unknown signal parameters and the modulation scheme being used. This can be seen to be a form of the well known Total Probability Theorem. While this likelihood-based approach is optimal for handling unknown signal parameters, it can be difficult, if not impossible, to develop due to the multi-dimensional integration required when handling multiple unknown signal parameters. Also, in the context of classifying signals in slowly varying flat-fading channels, [18] states that the multi-dimensional integration required results in an exponentially complex classifier for Rayleigh fading, while being mathematically intractable for other fading models (such as Rice, Weibull, and Nakagami).

Another composite hypothesis testing approach is the GLRT, in which the unknown parameters are considered to be deterministic and unknown. For this approach, maximum-likelihood estimates of the unknown parameters are found conditioned on each of the possible modulation schemes. Thus, the estimator is given by

$$\max_{H_i,\mathbf{u}} p(r(t)|\mathbf{u}, H_i) = \max_{H_i} \left\{ \max_{\mathbf{u}} p(r(t)|\mathbf{u}, H_i) \right\}. \tag{2.2}$$

Once these estimates are found, they are then utilized by the modulation classifier. This sub-optimal approach generally yields easier to implement classifiers than the ALRT-based approach. However, this method can still be difficult to implement when handling multiple unknown signal parameters, due to the multi-dimensional maximization required. Additionally, prior work has shown that the GLRT fails in uniquely classifying nested constellations (such as 16-QAM and 32-QAM) and thus may be inadequate for some classification problems of interest [21],[24].

The HLRT approach can be used to avoid some of the described modulation classification disadvantages of the ALRT and GLRT. For the HLRT, the classifier's dependence on the unknown

modulated data symbols is removed through (2.1) (as with the ALRT), while the unknown non-data signal parameters are estimated using maximum-likelihood estimation through (2.2) (as with the GLRT). This approach removes the need for multi-dimensional integration, while avoiding the nested constellation problem [21]. However, the inherent difficulty in performing multi-dimensional maximization is still present.

If a lower complexity estimation approach is used to estimate the unknown non-data signal parameters with the HLRT, as opposed to maximum-likelihood estimation, this is known as the quasi-Hybrid Likelihood Ratio Test (qHLRT). This approach removes the need for multi-dimensional integration and maximization, leading to lower complexity classifiers than each of the previous approaches, while still being able to provide performance comparable to the HLRT [19]. It is this approach that will be utilized in the development of the proposed asynchronous classifier. This approach is chosen due to its ease of use, and lower complexity requirements, over the other described approaches when dealing with multiple unknown non-data signal parameters.

2.4 The Asynchronous qHLRT-based Modulation Classifier

In this section, the asynchronous qHLRT-based modulation classifier for digital amplitude-phase modulated signals in slowly varying flat-fading channels is developed. The received signal is defined as

$$r(t) = \Re\left\{ \sum_{k=-\infty}^{\infty} S_k p(t-(\epsilon+\eta)T - kT)\alpha e^{j(2\pi f_c t+\theta)} \right\} + n(t) \qquad (-\infty < t < \infty), \tag{2.3}$$

where the symbol interval T, the carrier frequency f_c, and the real-valued pulse shape $p(t)$ are assumed known. The pulse shapes considered in this work are assumed to satisfy the Nyquist Intersymbol Interference (ISI) criterion and to be normalized to have unit energy. The term $n(t)$ represents a white Gaussian noise process with two-sided power spectral density $N_0/2$ W/Hz, where N_0 is also assumed known.

The unknown signal parameters are considered to be the modulated data symbols, the fading parameters α and θ, and the time delay parameters η and ϵ. The term S_k represents the k-th unknown modulated data symbol, taken from the set of complex constellation values of the modulation scheme being used. The unknown real-valued channel gain α and phase θ, due to the

assumption of a slowly varying flat-fading channel, are considered constant during the observation interval.

The unknown time delay, in symbol intervals, is represented by the two unknown parameters η and ϵ. The delay term η represents the integer number of symbol intervals delayed, while the delay term ϵ represents the remaining fractional symbol interval delayed ($0 \leq \epsilon < 1$). Thus, the unknown total time delay can be represented by $(\epsilon + \eta)T$.

The general synchronous receiver for signals of the form (2.3) can be seen in Fig. 2.1. Here, the term synchronous is defined as knowledge of the fractional time delay ϵ, with no knowledge of η assumed. This is a conventional matched filter receiver, in which the received signal is demodulated, correlated with the pulse shape $p(t)$, and sampled at the optimal sampling instant t_{opt} (defined to be the sampling instant at which no ISI is present). For the pulse shapes considered in this work, $t_{opt} = (n + \epsilon)T$.

From Appendix A, the output of this receiver is shown to be the complex point

$$r_{n,\epsilon} = c_{n,\epsilon} - j s_{n,\epsilon} = \frac{1}{2} S_{n-\eta} \alpha e^{j\theta} + noise_n. \tag{2.4}$$

From standard detection theory [25], the vector $\mathbf{r}_\epsilon = [c_{1,\epsilon} - j s_{1,\epsilon}, c_{2,\epsilon} - j s_{2,\epsilon}, ..., c_{N,\epsilon} - j s_{N,\epsilon}]$ is a set of sufficient statistics for the detection of the N symbols $S_{1-\eta}, S_{2-\eta}, \ldots, S_{N-\eta}$. Therefore, for the modulation classification problem given an observation length of N symbols, finding the maximum among $p(r(t)|H_i)$ is equivalent to finding the maximum among $p(\mathbf{r}_\epsilon|H_i)$ [15].

Assuming an observation length of N_c symbols, there are $M_i^{N_c}$ possible modulated data symbol sequences that can occur given the i-th modulation scheme, where M_i is the modulation scheme's cardinality. From the Total Probability Theorem,

$$p(\mathbf{r}_\epsilon|H_i) = \sum_{m=1}^{M_i^{N_c}} p(\mathbf{r}_\epsilon|\mathbf{s}_{m,i}, H_i) P(\mathbf{s}_{m,i}|H_i), \tag{2.5}$$

where the vector $\mathbf{s}_{m,i}$ is one of the $M_i^{N_c}$ possible modulated data symbol sequences of length N_c. More specifically, the set $\left\{\mathbf{s}_{1,i}, \mathbf{s}_{2,i}, \ldots, \mathbf{s}_{M_i^{N_c},i}\right\}$ corresponds to all possible modulated data symbol sequences of length N_c of the i-th modulation scheme. Given that the samples $r_{n,\epsilon}$ are independent (based on the assumptions that there is no ISI and that the noise $n(t)$ is white), $p(\mathbf{r}_\epsilon|H_i)$ can be

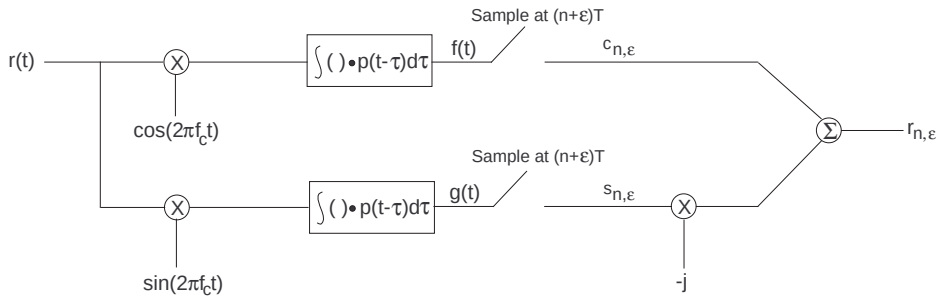

Figure 2.1: Conventional matched filter receiver for digital amplitude-phase modulated signals.

rewritten as

$$p(\mathbf{r}_\epsilon|H_i) = \prod_{n=1}^{N_c} \sum_{k=1}^{M_i} p(r_{n,\epsilon}|S_{k,i}, H_i) P(S_{k,i}|H_i), \tag{2.6}$$

where $S_{k,i}$ is one of the M_i possible complex constellation values of the i-th modulation scheme.

A final simplification can be made by assuming that all of the complex constellation values are equally likely. Taking the natural log of (2.6), and applying this final simplifying assumption, the maximum-likelihood classifier can be written as [15]

$$\hat{H} = \arg\max_{H_i} \sum_{n=1}^{N_c} \ln\left(\frac{1}{M_i}\sum_{k=1}^{M_i} p(r_{n,\epsilon}|S_{k,i}, H_i)\right), \tag{2.7}$$

where the probability $p(r_{n,\epsilon}|S_{k,i}, H_i)$ is determined in Appendix A. Combining equations (2.7) and (A.12),

$$\hat{H} = \arg\max_{H_i} \sum_{n=1}^{N_c} \ln\left\{\frac{1}{M_i}\sum_{k=1}^{M_i} e^{-\frac{2}{N_0}|r_{n,\epsilon}-\frac{1}{2}\alpha e^{j\theta}S_{k,i}|^2}\right\}, \tag{2.8}$$

where the terms common to each argument have been removed.

Finally, based on the qHLRT-based classification approach, the assumed unknown parameters α, θ, and ϵ are replaced by their estimates (denoted by $\hat{}$). This leads to the final form of

$$\hat{H} = \arg\max_{H_i} \sum_{n=1}^{N_c} \ln\left\{\frac{1}{M_i}\sum_{k=1}^{M_i} e^{-\frac{2}{N_0}|r_{n,\hat{\epsilon}}-\frac{1}{2}\hat{\alpha} e^{j\hat{\theta}}S_{k,i}|^2}\right\} \tag{2.9}$$

for the proposed asynchronous qHLRT-based modulation classifier, where $r_{n,\hat{\epsilon}}$ is the output of the receiver in Fig. 2.1 given the sampling instant $(n+\hat{\epsilon})T$.

2.5 Estimation of the Unknown Non-data Signal Parameters

Now that the proposed asynchronous qHLRT-based modulation classifier has been described, the focus of this section is to present the development of the low complexity estimators used to estimate the unknown non-data signal parameters α, θ, and ϵ. The major constraint on these estimators is that they must estimate the parameters of interest with *no prior knowledge* of the modulation scheme of the received signal (i.e. such benefits as training sequences are not available). Minding this constraint, the estimators in this work are developed using an estimation approach known as the Method-of-Moments (MoM).

The MoM is an estimation process in which unknown parameters are estimated through the solution of a system of statistical moment equations. These statistical moment equations are in turn defined from a known pdf that is a function of the unknown parameters. MoM estimators, while sub-optimal, are usually much easier to implement than optimal maximum-likelihood estimators [26]. As an example application of their use in modulation classification, a *synchronous* qHLRT-based classifier for digital amplitude-phase modulated signals in flat-fading channels was developed in [19], where MoM estimates of α, θ, and N_0 were used by the classifier. It is shown in [19] that, given an adequate observation interval, the resulting classifier's performance is comparable to that of a classifier using maximum-likelihood estimates.

A major contribution of this chapter is the development of a *novel* MoM based estimator for α and ϵ that is blind to the modulation scheme of the received signal. Therefore, the majority of the discussion presented in the following will be on the development and performance of this estimator, as well as its applications to the proposed asynchronous qHLRT-based modulation classifier.

2.5.1 General Formulation of the MoM-based Estimator for the Unknown Channel Gain and Fractional Time Delay

It will be shown in this section that a novel MoM-based estimator can be developed for the unknown parameters α and ϵ through the use of the three moments $M_{\lambda_1} = E[|r_{n,\lambda_1}|^2]$, $M_{\lambda_2} = E[|r_{n,\lambda_2}|^2]$, and $M_{\lambda_3} = E[|r_{n,\lambda_3}|^2]$. These moments will be defined in general for any arbitrary pulse shape that satisfies the Nyquist ISI criterion, and will be defined specifically for the rectangular and square

root-raised cosine pulse shapes in Sections 2.5.2 and 2.5.3, respectfully. From these developments, it will be shown that the moments are a function of only the unknown signal parameters α and ϵ, while not being a function of the parameters n, η and θ.

To begin this development, the first step is to define the set of moment equations to be used. To do this, it is first assumed that the output of the matched filter in Fig. 2.1 is sampled at $t_{n,\lambda_1} = (n+\lambda_1)T$, where n is an integer and λ_1 is an arbitrarily chosen value with range $0 \leq \lambda_1 < 1$. It is important to note that the chosen value λ_1 is not dependent in any way on the unknown time delay parameters ϵ and η; it simply defines a sampling time for the output of the matched filter receiver.

From (A.7), the output of the receiver given the sampling time t_{n,λ_1} is

$$r_{n,\lambda_1} = \frac{1}{2}\alpha e^{j\theta} \sum_{k=-\infty}^{\infty} \{S_k R(t_{n,\lambda_1})\} + noise_n, \tag{2.10}$$

where

$$R(t_{n,\lambda_1}) = \int_{-\infty}^{\infty} p(\tau - (\epsilon+\eta)T - kT)p(t_{n,\lambda_1} - \tau)d\tau. \tag{2.11}$$

Given (2.10), the first moment of interest is defined as

$$\begin{aligned} M_{\lambda_1} &= E[|r_{n,\lambda_1}|^2] = E\left[\left|\frac{1}{2}\alpha e^{j\theta} \sum_{k=-\infty}^{\infty} \{S_k R(t_{n,\lambda_1})\} + noise_n\right|^2\right] \\ &= \frac{\alpha^2}{4}\left\{\sum_{k=-\infty}^{\infty} E[|S_k|^2] R(t_{n,\lambda_1})^2\right\} + \frac{N_0}{2} \\ M_{\lambda_1} &= \frac{\alpha^2}{4}\psi_{\lambda_1} + \frac{N_0}{2}, \end{aligned} \tag{2.12}$$

with

$$\psi_{\lambda_1} = \sum_{k=-\infty}^{\infty} R(t_{n,\lambda_1})^2, \tag{2.13}$$

assuming that the modulated data symbols are independent and from a symmetric modulation scheme that is normalized to unit average power (i.e. $E[\Re\{S_k\}] = 0$, $E[\Im\{S_k\}] = 0$, and $E[|S_k|^2] = 1$). Given that $t_{n,\lambda_1} = (n+\lambda_1)T$, the term ψ_{λ_1} is given by

$$\psi_{\lambda_1} = \sum_{m=-\infty}^{\infty} \left\{\int_{-\infty}^{\infty} p(\tau)p(mT + (\lambda_1 - \epsilon)T - \tau)d\tau\right\}^2. \tag{2.14}$$

Based on (2.14), it is worth noting that the moment equation (2.12) is a function of the unknown parameters α and ϵ, while not being a function of the parameters n, η, or θ.

Expanding on this idea to determine the next moment of interest, assume that the receiver now has a sampling time of $t_{n,\lambda_2} = (n + \lambda_2)T$, where λ_2 is a second arbitrarily chosen value with range $0 \leq \lambda_2 < 1$ ($\lambda_2 \neq \lambda_1$). Based on this new sampling time, a second moment defined equivalently by (2.12) can be determined ($M_{\lambda_2} = E[|r_{n,\lambda_2}|^2]$). Note that each of the moments M_{λ_1} and M_{λ_2} are a function of the same unknown parameters α and ϵ. Therefore, these moment equations can be solved in terms of α and set equivalent, resulting in an equation that is only a function of the unknown parameter ϵ. Therefore,

$$\alpha = \sqrt{\frac{2(2M_{\lambda_1} - N_0)}{\psi_{\lambda_1}}} = \sqrt{\frac{2(2M_{\lambda_2} - N_0)}{\psi_{\lambda_2}}} \tag{2.15}$$

$$\underbrace{\frac{2M_{\lambda_1} - N_0}{2M_{\lambda_2} - N_0}}_{\text{Moment Term}} - \underbrace{\frac{\psi_{\lambda_1}}{\psi_{\lambda_2}}}_{\text{Variable Term}} = 0. \tag{2.16}$$

In (2.16), two terms of interest have been labeled, the moment term and the variable term. The moment term is a function of the moments M_{λ_1} and M_{λ_2}, as well as the known noise parameter N_0. The variable term is a function of the known pulse shape $p(t)$, the chosen values λ_1 and λ_2, and the unknown fractional time delay ϵ. Therefore, if the moments can be determined, estimates for the unknown fractional time delay can be found by finding the zero crossings of (2.16) as a function of ϵ. These estimates can then in turn be used to determine the possible estimates for the unknown channel gain α through (2.15).

It will be shown for the pulse shapes considered in this work, rectangular and square root-raised cosine, that it is possible to find up to two zero-crossings in (2.16). When more than one zero-crossing is found, an estimation ambiguity exists in which there is more than one possible estimate for the fractional time delay ϵ. To resolve this ambiguity, an additional moment $M_{\lambda_3} = E[|r_{n,\lambda_3}|^2]$ can be determined, where λ_3 is a third arbitrarily chosen value with $0 \leq \lambda_3 < 1$ and $\lambda_1 \neq \lambda_2 \neq \lambda_3$. This additional moment can be used with each of the moments M_{λ_1} and M_{λ_2} equivalently in the zero-finding equation (2.16) to resolve the estimation ambiguity. This process will be discussed in more detail in the following.

In practice, the moments M_{λ_i} are unknown *a priori* and thus must be estimated from the received

signal. This is done through the use of the sample average of the matched filter outputs, defined as

$$\hat{M}_{\lambda_i} = \frac{1}{N_{est}} \sum_{n=n_i}^{n_i+N_{est}} |r_{n,\lambda_i}|^2, \tag{2.17}$$

where r_{n,λ_i} is the matched filter output given the sampling time $t_{n,\lambda_i} = (n+\lambda_i)T$, N_{est} is the number of outputs observed, and n_i is an arbitrary integer ($n_i = 0$ in Fig. 2.1). It is readily understood that any estimation error in the estimates of the moments will directly effect the reliability of the estimates of the unknown parameters α and ϵ. Therefore, the more accurately these moments are estimated, the better the accuracy of the α and ϵ estimates.

To summarize, the following steps define the proposed MoM-based estimator for α and ϵ:

1. Given the chosen values $\lambda_1, \lambda_2,$ and λ_3, determine the moment estimates $\hat{M}_{\lambda_1}$, $\hat{M}_{\lambda_2}$, and $\hat{M}_{\lambda_3}$ using the sample average estimator defined by (2.17).

2. For each possible pair of moments ($[\hat{M}_{\lambda_1}, \hat{M}_{\lambda_2}]$, $[\hat{M}_{\lambda_1}, \hat{M}_{\lambda_3}]$, and $[\hat{M}_{\lambda_2}, \hat{M}_{\lambda_3}]$), determine the zero-crossings of (2.16). The corresponding zero-crossings are the fractional time delay estimates $\hat{\epsilon}$. (The term $\hat{\epsilon}$ represents an imperfect estimate of the fractional time delay, due to the moments being estimates and thus containing error.)

3. Determine the $\hat{\epsilon}$ values (one from each moment pair) that most closely agree. Save these estimates and discard the remaining.

4. Using the saved $\hat{\epsilon}$ values, determine the corresponding amplitude estimates $\hat{\alpha}$ through (2.15).

5. Determine the final estimation values based upon the set of determined $\hat{\epsilon}$ and $\hat{\alpha}$ values.

In the following sections, the proposed MoM-based estimator for α and ϵ is discussed for two pulse shapes of interest: rectangular and square root-raised cosine. In the performance analysis presented in these sections, and in the modulation classification performance analysis in Section 2.6, the estimates $\hat{\alpha}$ and $\hat{\epsilon}$ are determined through the use of the moments $M_{\lambda_1=0}$, $M_{\lambda_2=1/3}$, and $M_{\lambda_3=2/3}$. In Step 1 of the estimation process defined above, these moments are estimated using N_{est} uncorrelated, with regards to the noise, r_{n,λ_i} values ($i = 1, 2, 3$ and $n = n_i, n_i+1, \ldots, n_i+(N_{est}-1)$). For Step 2 of the estimation process, the possible fractional time delay estimates are determined

from (2.16) through the well known Bisection Method of zero-finding [27]. Given the possible time delay estimates found from Step 2, the $\hat{\epsilon}$ estimates saved in Step 3 are chosen as the set of estimates (one from each moment pair) that have the smallest standard deviation between the estimates in the set. Finally, for Step 5, the final estimates $\hat{\alpha}$ and $\hat{\epsilon}$ are determined by taking the mean of the saved sets found from Steps 3 and 4.

2.5.2 Estimation given a Rectangular Pulse Shape

In this section, the performance of the proposed MoM-based α and ϵ estimator is analyzed under the assumption that the received signal, defined by (2.3), utilizes the rectangular pulse shape defined by

$$p(t) = \begin{cases} \frac{1}{\sqrt{T}} & \text{for } -\frac{T}{2} \leq t \leq \frac{T}{2} \\ 0 & \text{otherwise} \end{cases}. \tag{2.18}$$

For this pulse shape, the matched filter receiver output (2.10), given the sampling time $t_{n,\lambda_i} = (n+\lambda_i)T$, is shown to be

$$\begin{aligned} r_{n,\lambda_i} &= \frac{1}{2}\alpha e^{j\theta} \sum_{k=-\infty}^{\infty} \{S_k R(t_{n,\lambda_i})\} + noise_n \\ &= \frac{1}{2}\alpha e^{j\theta} \sum_{k=-\infty}^{\infty} \left\{ S_k \int_{-\infty}^{\infty} p(\tau - (\epsilon+\eta)T - kT) p(t_{n,\lambda_i} - \tau) d\tau \right\} + noise_n \\ r_{n,\lambda_i} &= \frac{1}{4}|\epsilon - \lambda_i| \alpha e^{j\theta} (S_{n-\eta-1} - 2S_{n-\eta} + S_{n-\eta+1}) \\ &\quad + \frac{1}{4}\alpha e^{j\theta} (S_{n-\eta-1}(\epsilon - \lambda_i) + 2S_{n-\eta} + S_{n-\eta+1}(\lambda_i - \epsilon)) + noise_n. \end{aligned} \tag{2.19}$$

(It is worth nothing that (2.19) reduces to the optimal matched filter receiver output (A.9) given $\epsilon = \lambda_i$.)

Given (2.19), the moments $M_{\lambda_i} = E[|r_{n,\lambda_i}|^2]$ can be shown to be defined by

$$\begin{aligned} M_{\lambda_i} &= \Big(-\alpha^2 \left(\frac{\epsilon}{2} - \frac{\lambda_i}{2} \right) E[|S_{n-\eta}|^2] - \alpha^2 \left(\frac{\epsilon^2}{8} - \frac{\epsilon\lambda_i}{4} + \frac{\lambda_i^2}{8} \right) E[|S_{n-\eta+1}|^2] \\ &\quad + \alpha^2 \left(\frac{\epsilon^2}{8} - \frac{\epsilon\lambda_i}{4} + \frac{\lambda_i^2}{8} \right) E[|S_{n-\eta-1}|^2] \Big) sign(\epsilon - \lambda_i) \\ &\quad + \alpha^2 \left(\frac{\epsilon^2}{4} - \frac{\epsilon\lambda_i}{2} + \frac{\lambda_i^2}{4} + \frac{1}{4} \right) E[|S_{n-\eta}|^2] + \alpha^2 \left(\frac{\epsilon^2}{8} - \frac{\epsilon\lambda_i}{4} + \frac{\lambda_i^2}{8} \right) E[|S_{n-\eta+1}|^2] \\ &\quad + \alpha^2 \left(\frac{\epsilon^2}{8} - \frac{\epsilon\lambda_i}{4} + \frac{\lambda_i^2}{8} \right) E[|S_{n-\eta-1}|^2] + \frac{N_0}{2}, \end{aligned} \tag{2.20}$$

assuming that the modulated data symbols are independent and from a symmetric modulation scheme. If a further assumption is made that the modulation schemes are normalized to unit average power (i.e. $E[|S_{n-\eta-1}|^2 = 1$, $E[|S_{n-\eta}|^2 = 1$, and $E[|S_{n-\eta+1}|^2 = 1)$, (2.20) can be reduced to the simplified form

$$M_{\lambda_i} = \frac{\alpha^2}{4} \underbrace{\left[1 - 2|\epsilon - \lambda_i| + 2(\epsilon - \lambda_i)^2\right]}_{\psi_{\lambda_i}} + \frac{N_0}{2}, \tag{2.21}$$

where solving for α leads to

$$\alpha = \sqrt{\frac{2(2M_{\lambda_i} - N_0)}{1 - 2|\epsilon - \lambda_i| + 2(\epsilon - \lambda_i)^2}}. \tag{2.22}$$

(Note that (2.21) is not a function of the unknown parameter η.)

Finally, given the two moments M_{λ_i} and M_{λ_j} $(i \neq j)$, the zero-finding equation of (2.16) can be shown to be defined as

$$\underbrace{\frac{2M_{\lambda_i} - N_0}{2M_{\lambda_j} - N_0}}_{\text{Moment Term}} - \underbrace{\frac{1 - 2|\epsilon - \lambda_i| + 2(\epsilon - \lambda_i)^2}{1 - 2|\epsilon - \lambda_j| + 2(\epsilon - \lambda_j)^2}}_{\text{Variable Term}} = 0. \tag{2.23}$$

It is worth reiterating that the moments M_{λ_i} and M_{λ_j} of (2.23) are not known *a priori* and thus must be estimated using the sample average estimator defined by (2.17).

In Fig. 2.2, the variable term of (2.23) can be seen for different sets of λ_i and λ_j values. One important observation that can be made from this figure is that, for a given value of the variable term, there can be up to two possible values for the unknown fractional time delay ϵ (note that only one solution exists when $\epsilon = \lambda_i$ or $\epsilon = \lambda_j$). In regards to the proposed estimator, this can result in what has been defined in Section 2.5.1 as an estimation ambiguity. Another important observation that can be made from Fig. 2.2 is the effect of the choice of the chosen values λ_i and λ_j on the variable term. As the "minimum distance" between these values increases (defined as the minimum between the distance $(\lambda_j - \lambda_i)$ and the wrap around distance $((1 - \lambda_j) + \lambda_i)$, $\lambda_j > \lambda_i)$, so does the range of the variable term.

Under the assumption of a rectangular pulse shape, Figs. 2.3-2.5 present performance results of the proposed α and ϵ estimator using the estimation process defined in Section 2.5.1. For these performance results, the modulation schemes considered are BPSK, QPSK, 8-PSK, 16-QAM, and 64-QAM, with the modulation schemes considered to be normalized to unit average power. Also,

the fading model is assumed to be Rayleigh, and the average power of α is assumed to be unity ($E[\alpha^2] = 1$).

These plots show the proposed estimator's performance as a function of both the SNR, defined here as $\frac{E[\alpha^2]}{2N_0}$, and N_{est}. In Fig 2.3, it can be observed that as the SNR and/or N_{est} is increased, the probability of estimation failure decreases. An estimation failure is defined to be when the estimator fails to find an unambiguous estimate for the unknown fractional time delay ϵ (meaning that zero-crossings can not be determined for two or more of the three possible zero-finding equations). Given that an estimation failure does not occur, Figs. 2.4 and 2.5 present the average mean square error (AMSE) of the estimates $\hat{\epsilon}$ and $\hat{\alpha}$, respectively. For these results, the AMSE is defined as

$$AMSE = \frac{1}{N_m} \sum_{i=1}^{N_m} E[|\hat{x}_i - x|^2], \tag{2.24}$$

where x is the parameter being estimated and N_m is the total number of modulation schemes assumed. As expected, as the SNR and/or N_{est} increases, the average mean square error of the estimates decreases.

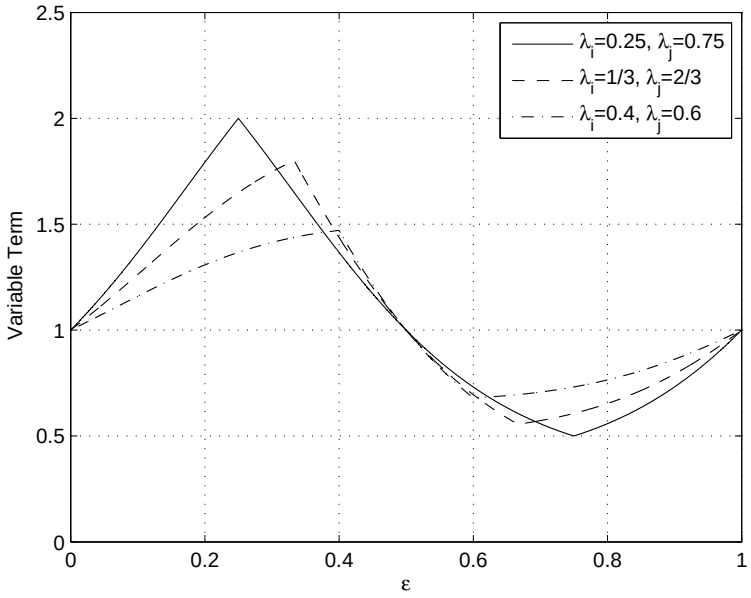

Figure 2.2: Variable term given a rectangular pulse shape.

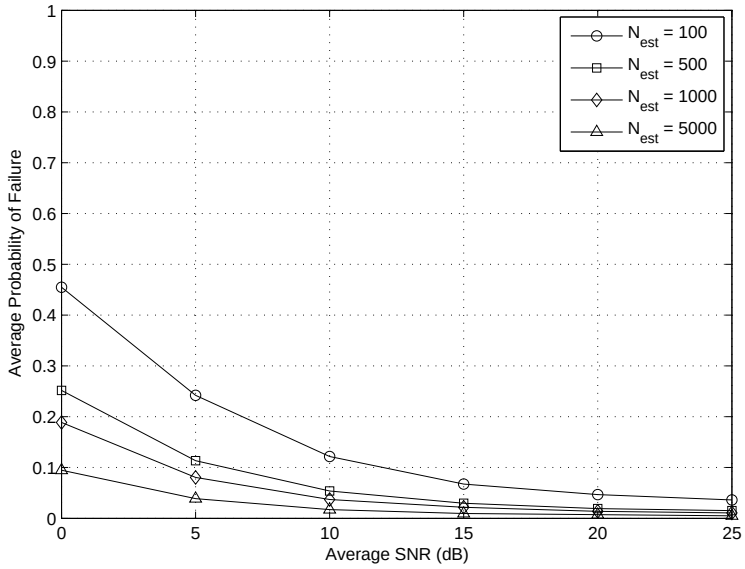

Figure 2.3: Average probability of estimation failure given a rectangular pulse shape.

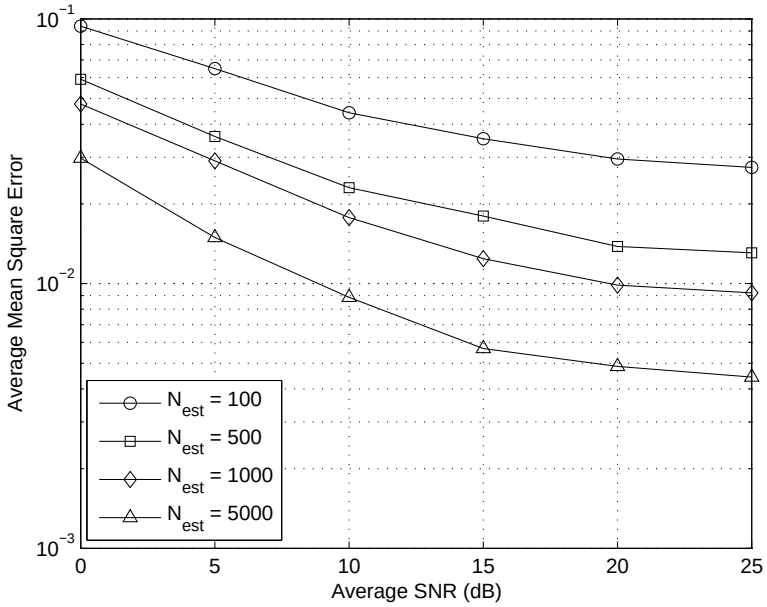

Figure 2.4: Average mean square error of $\hat{\epsilon}$ given a rectangular pulse shape.

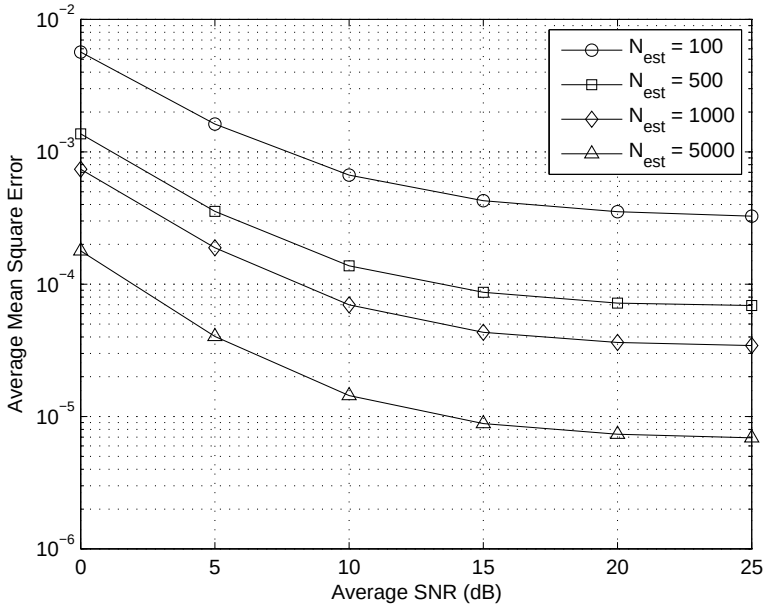

Figure 2.5: Average mean square error of $\hat{\alpha}$ given a rectangular pulse shape.

2.5.3 Estimation given a Square Root-Raised Cosine Pulse Shape

In this section, the performance of the proposed MoM-based α and ϵ estimator is analyzed under the assumption that the received signal, defined by (2.3), utilizes the square root-raised cosine pulse shape defined by

$$p(t) = \frac{4\beta}{\pi\sqrt{T}} \frac{\cos((1+\beta)\pi\frac{t}{T}) + \frac{\sin((1-\beta)\pi\frac{t}{T})}{4\beta\frac{t}{T}}}{1-(4\beta\frac{t}{T})^2} \qquad (-\infty < t < \infty), \tag{2.25}$$

where $P(f) = |P_{RC}(f)|^{\frac{1}{2}}$, $P_{RC}(f)$ is the frequency domain representation of the raised cosine pulse shape $p_{RC}(t)$, and β is the roll-off factor.

For this pulse shape, the matched filter receiver output (2.10), given the sampling time $t_{n,\lambda_i} = (n+\lambda_i)T$, is shown to be

$$\begin{aligned}
r_{n,\lambda_i} &= \frac{\alpha e^{j\theta}}{2} \sum_{k=-\infty}^{\infty} \{S_k R(t_{n,\lambda_i})\} + noise_n \\
&= \frac{\alpha e^{j\theta}}{2} \sum_{k=-\infty}^{\infty} \left\{ S_k \int_{-\infty}^{\infty} p(\tau - (\epsilon+\eta)T - kT) p(t_{n,\lambda_i} - \tau) d\tau \right\} + noise_n \\
r_{n,\lambda_i} &= \frac{\alpha e^{j\theta}}{2} \sum_{k=-\infty}^{\infty} \left\{ S_k \underbrace{\left[\frac{\cos(\pi\beta[(\lambda_i-\epsilon)+(n-\eta-k)])}{1-(2\beta[(\lambda_i-\epsilon)+(n-\eta-k)])^2} \frac{\sin(\pi[(\lambda_i-\epsilon)+(n-\eta-k)])}{\pi[(\lambda_i-\epsilon)+(n-\eta-k)]} \right]}_{p_{RC}([(\lambda_i-\epsilon)+(n-\eta-k)]T)} \right\} \\
&\quad + noise_n.
\end{aligned} \tag{2.26}$$

(As was the case when considering a rectangular pulse shape, (2.26) reduces to the optimal matched filter receiver output (A.7) if $\epsilon = \lambda_i$.)

Given (2.26), the moments $M_{\lambda_i} = E[|r_{n,\lambda_i}|^2]$ can be shown to be defined by

$$M_{\lambda_i} = \frac{\alpha^2}{4} \underbrace{\left\{ \sum_{m=-\infty}^{\infty} p_{RC}([(\lambda_i-\epsilon)+m]T)^2 \right\}}_{\psi_{\lambda_i}} + \frac{N_0}{2}, \tag{2.27}$$

assuming independent modulated data symbols from a symmetric modulation scheme that is normalized to unit average power. Furthermore, solving for α in (2.27) results in

$$\alpha = \sqrt{\frac{2(2M_{\lambda_i} - N_0)}{\sum_{m=-\infty}^{\infty} p_{RC}([(\lambda_i-\epsilon)+m]T)^2}}, \tag{2.28}$$

which can be observed to not be a function of the unknown parameter η.

Finally, given the two moments M_{λ_i} and M_{λ_j} $(i \neq j)$, the zero-finding equation of (2.16) can be shown to be defined as

$$\underbrace{\frac{2M_{\lambda_i} - N_0}{2M_{\lambda_j} - N_0}}_{\text{Moment Term}} - \underbrace{\frac{\sum_{m=-\infty}^{\infty} p_{RC}([(\lambda_i - \epsilon) + m]T)^2}{\sum_{m=-\infty}^{\infty} p_{RC}([(\lambda_j - \epsilon) + m]T)^2}}_{\text{Variable Term}} = 0. \tag{2.29}$$

Again, note that the moments M_{λ_i} and M_{λ_j} of (2.29) are not known *a priori* and thus must be estimated using the sample average estimator defined by (2.17).

Fig. 2.6 presents plots of the variable term of (2.29) for different sets of λ_i, λ_j, and β values. As was shown for a rectangular pulse shape, it can be observed that for a given value of the variable term there can be up to two possible values for the unknown fractional time delay parameter ϵ. Again, this can result in what has been defined in Section 2.5.1 as an estimation ambiguity.

It can also be observed from Fig. 2.6 that there are two factors that determine the range of the variable term. The first of these factors is the so-called "minimum distance" that was previously described for the rectangular pulse shape. The second factor is the roll-off factor β. It can be seen that a decrease in β increases the side lobes of the pulse shape, which in turn effects the summations of (2.29), causing the range of the variable term to decrease.

Under the same simulation conditions assumed given a rectangular pulse in Section 2.5.2, Figs. 2.7-2.9 present performance results of the proposed α and ϵ estimator given a square root-raised cosine pulse shape with roll-off factor $\beta = 0.75$. From these figures, the same trends in the performance of the estimator can be observed given this square root-raised cosine pulse shape as was observed in the previous section given a rectangular pulse shape. For instance, as the SNR and/or N_{est} increases, the average probability of estimation failure decreases, as does the AMSE of the estimates $\hat{\alpha}$ and $\hat{\epsilon}$.

2.5.4 The M-power Phase Synchronizer

For the proposed classification method, the well known MoM-based M-power phase synchronizer is used in order to estimate the unknown phase θ [28]. The M-power phase synchronizer estimates

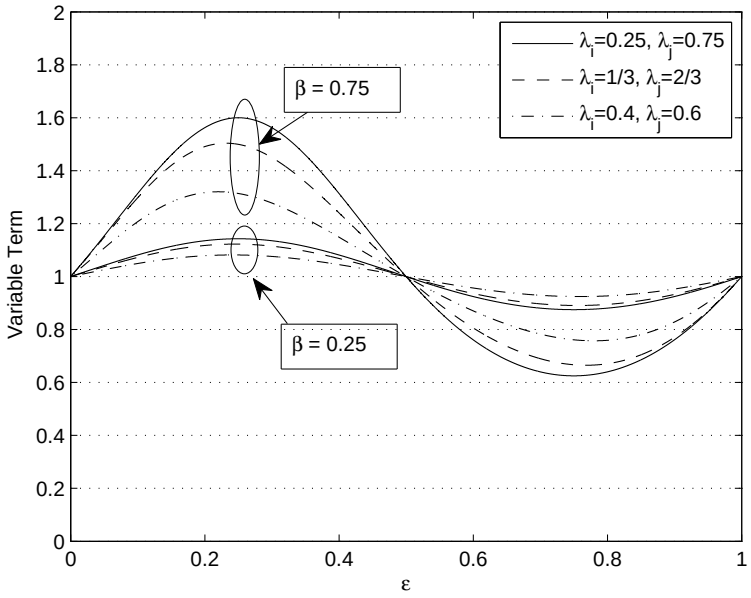

Figure 2.6: Variable term given a square root-raised cosine pulse shape.

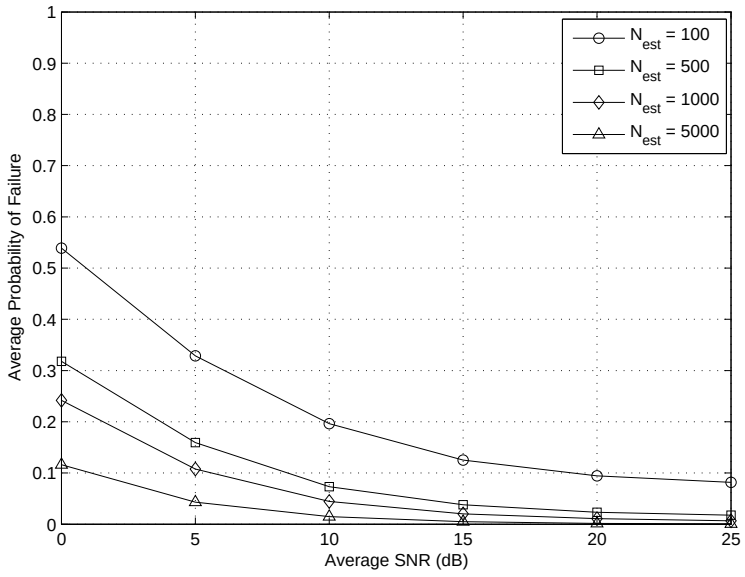

Figure 2.7: Average probability of estimation failure given a square root-raised cosine pulse shape ($\beta = 0.75$).

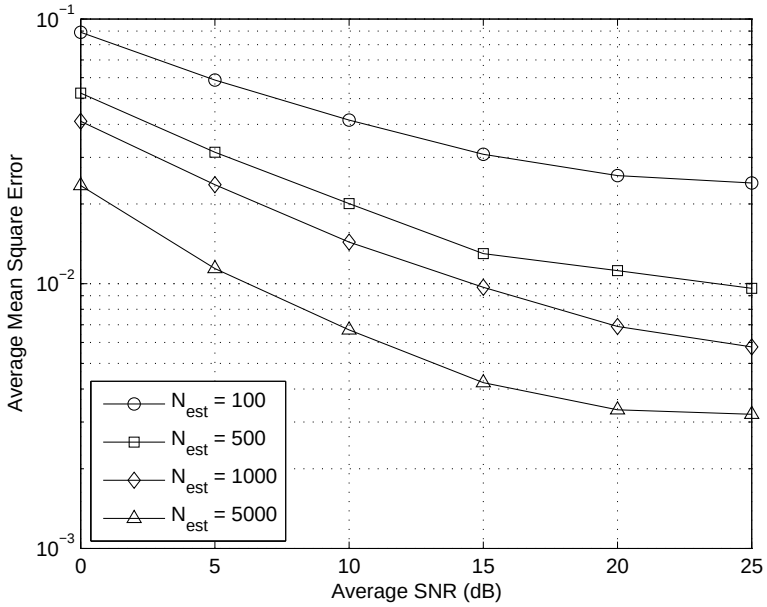

Figure 2.8: Average mean square error of $\hat{\epsilon}$ given a square root-raised cosine pulse shape ($\beta = 0.75$).

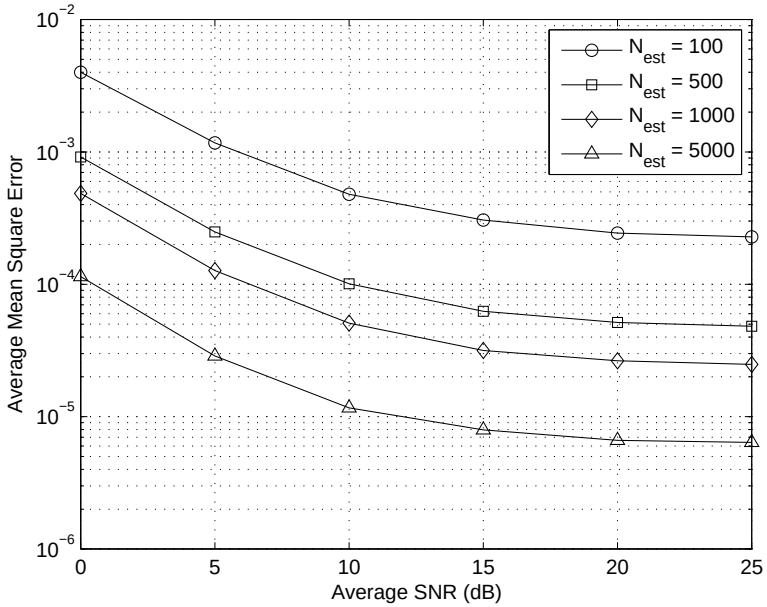

Figure 2.9: Average mean square error of $\hat{\alpha}$ given a square root-raised cosine pulse shape ($\beta = 0.75$).

θ through the use of a sample average estimator of the M-th moment of the receiver outputs $r_{n,\hat{\epsilon}}$ $(n = 1, 2, \ldots, N_c)$, where M is chosen based upon the modulation scheme assumed.

For PSK modulation schemes, the estimator is defined as

$$\hat{\theta}_{M-PSK} = \frac{1}{M}\arg\left\{\sum_{n=1}^{N_c} r_{n,\hat{\epsilon}}^{M}\right\}, \tag{2.30}$$

where M is the order of the PSK modulation scheme assumed. For QAM modulation schemes, the estimator is defined as

$$\hat{\theta}_{QAM} = \frac{1}{4}\arg\left\{\sum_{n=1}^{N_c} r_{n,\hat{\epsilon}}^{4}\right\}, \tag{2.31}$$

where $M = 4$ for all order of QAM schemes.

It should be mentioned that the phase estimates based upon the M-power phase synchronizer will have an M-fold phase ambiguity [28]. This is due to the fact that the arg function only gives values between $-\pi$ and π, restricting the phase estimates to the range $-\pi/M$ to π/M. However, for symmetric modulation schemes, such as the schemes considered in this work, this phase ambiguity will not result in a performance loss for the classification problem.

2.6 Performance Analysis of the Proposed Classifier

Fig. 2.10 presents the proposed asynchronous modulation classification system for digital amplitude-phase modulated signals in flat-fading channels. In this system, the unknown parameters α and ϵ are first estimated using the proposed MoM-based estimation process described in Section 2.5.1. Based on the estimated fractional time delay $\hat{\epsilon}$, the received signal is then demodulated and sampled to give the receiver outputs $r_{n,\hat{\epsilon}}$. These outputs are then used by the M-power phase synchronizer, discussed in Section 2.5.4, to provide the phase estimate $\hat{\theta}$. Finally, this phase estimate, along with $\hat{\alpha}$ and $r_{n,\hat{\epsilon}}$, is used to classify the received signal through the qHLRT-based modulation classifier defined by (2.9).

Figs. 2.11 and 2.12 present performance results of the proposed modulation classification system under the assumption that the pulse shape $p(t)$ is given by a rectangular pulse and a square root-raised cosine pulse, respectively. In this analysis, the modulation schemes considered are BPSK,

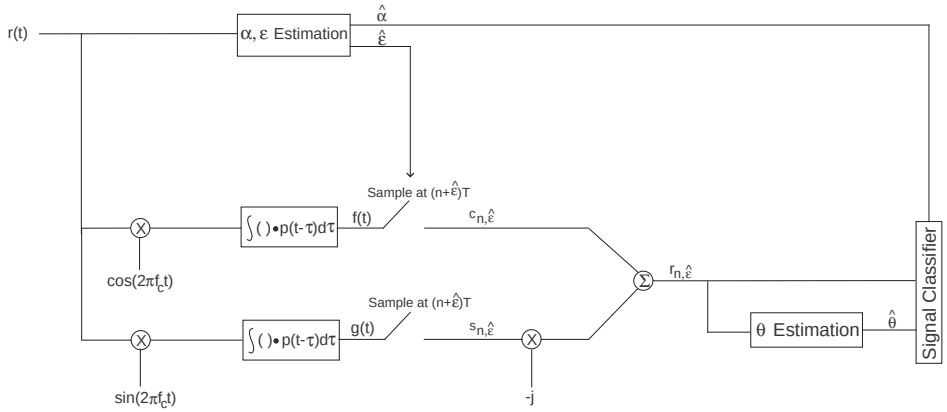

Figure 2.10: The proposed asynchronous modulation classification system.

QPSK, 8-PSK, 16-QAM, and 64-QAM, all with signal constellations normalized to have unit average power. The fading model is assumed to be Rayleigh and the average power of α is assumed to be unity ($E[\alpha^2] = 1$). The two values N_c and N_{est} respectively represent the number of terms used in the estimation of the unknown phase θ and the unknown parameters α and ϵ. Additionally, the value N_c is the number of $r_{n,\hat{\epsilon}}$ values used in the classification of the received signal.

These figures present the performance of the proposed classification system through the average probability of correct classification. For this analysis, a classification error is defined as one of two events: the proposed MoM-based estimator fails[2], or the classifier, if no estimation failure has occurred, decides upon an incorrect modulation scheme. As can be observed from these figures, the effect of increasing N_{est} on the performance of the proposed classifier can be quite substantial. This is due to the fact that, as N_{est} is increased, the estimates $\hat{\alpha}$ and $\hat{\epsilon}$ become more reliable (as was shown in the performance plots of Section 2.5.1), thus improving the overall performance of the classifier. Furthermore, for adequate values of N_{est}, the performance of the proposed classifier can be observed to approach that of the classifier in which the unknown signal parameters are assumed to be perfectly known.

[2]As previously stated, an estimation failure is defined to be when the estimator fails to find an unambiguous estimate for the unknown fractional time delay ϵ (meaning that zero-crossings can not be determined for two or more of the three possible zero-finding equations).

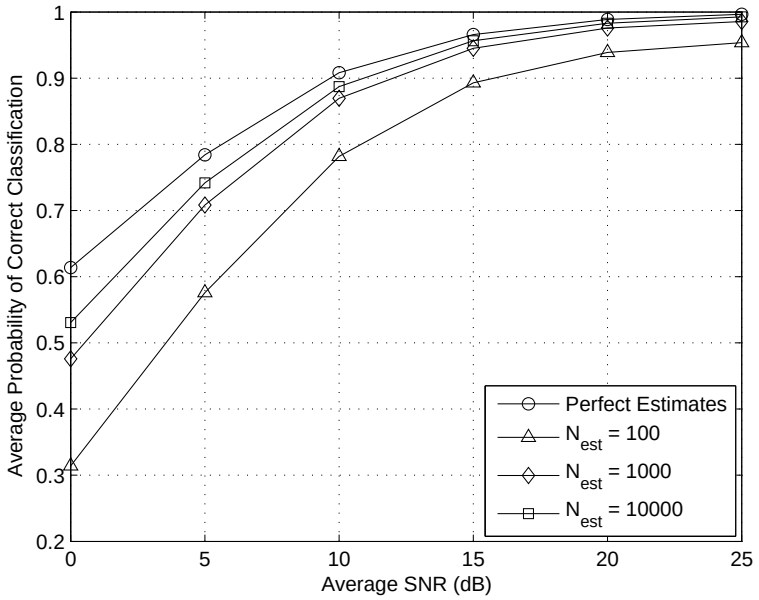

Figure 2.11: Average probability of correct classification given a rectangular pulse shape ($N_c = 500$).

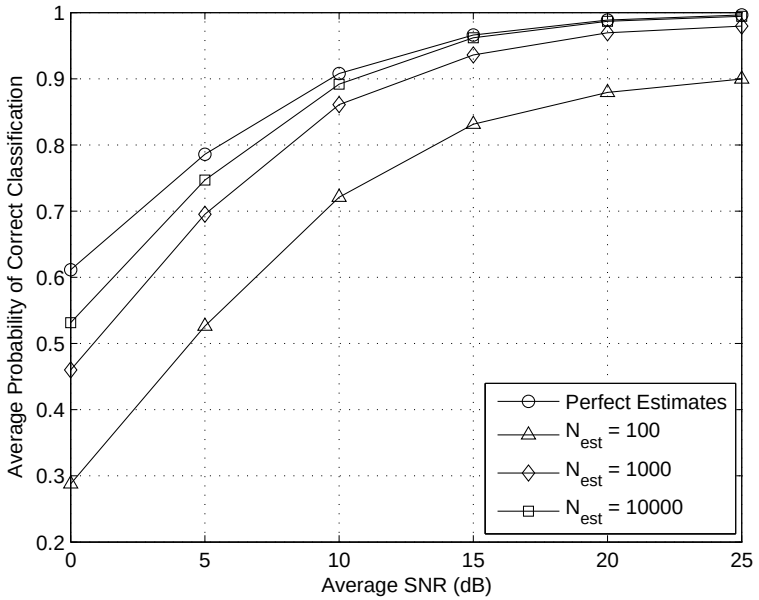

Figure 2.12: Average probability of correct classification given a square root-raised cosine pulse shape ($N_c = 500$ and $\beta = 0.75$).

2.7 Conclusions

In this chapter, a novel *asynchronous* and *noncoherent* classifier for digital amplitude-phase modulated signals in flat-fading channels was proposed. This classifier utilizes a likelihood-based approach known as the quasi-Hybrid Likelihood Ratio Test, in which estimates of the unknown non-data signal parameters are required. These unknown parameters were considered to be the channel gain, phase, and fractional time delay.

To provide these estimates, low complexity estimators based upon the method-of-moments were utilized that were shown to require no prior knowledge of the modulation scheme of the received signal. For the unknown channel gain and fractional time delay, a novel method-of-moments based estimator was proposed. Performance plots were then presented for this proposed estimator given two pulse shapes of interest, rectangular and square root-raised cosine. For the unknown phase, the well known method-of-moments based estimator known as the M-Power Phase Synchronizer was used.

Finally, performance results were presented for the proposed classifier for the two pulse shapes considered. These performance results demonstrate that the proposed asynchronous modulation classifier performs well compared to previously developed synchronous modulation classifiers, given an adequate observation interval.

Chapter 3

Asynchronous SNR Estimation of Digital Amplitude-Phase Modulated Signals in Flat-Fading Channels

3.1 Motivation for Work

The majority of prior work in signal-to-noise ratio estimation has made use of fairly strong assumptions concerning *a priori* knowledge of the received signal. For instance, many estimators assume knowledge of the modulation scheme utilized by the signal, or more stringently, knowledge of the transmitted set of modulated data symbols (usually through the use of training sequences) [29]-[31]. Even more universally, perfect time synchronization between the transmitter and receiver is almost always assumed [29]-[33].

While these common assumptions may be applicable in cooperative environments, this is not the case in non-cooperative environments. For instance, in environments employing cognitive radios [34],[35], it is likely that little information will be known about the neighboring signals (such as non-cooperative primary users or other secondary cognitive radio users). In such an application, the estimation of the signal-to-noise ratio can be of particular importance as a means of interference avoidance, for instance. With this in mind, the goal of the work presented in this chapter is to

remove some of these common assumptions through the development of an *asynchronous* signal-to-noise ratio estimator that *does not* require prior knowledge of the type of digital amplitude-phase modulation scheme used.

3.2 Contribution

In this chapter, an *asynchronous*, *noncoherent*, and *non-data-aided* signal-to-noise ratio estimator is developed for digital amplitude-phase modulated signals in flat-fading channels; in which no prior knowledge of the modulation scheme of the received signal is assumed. The proposed estimator utilizes a method-of-moments based approach similar to that of the estimator developed in Section 2.5 for estimating unknown channel gain and fractional time delay. Performance results are presented for the proposed estimator, assuming the use of both rectangular and square root-raised cosine pulse shapes, that demonstrate the performance capabilities of the estimator.

3.3 Signal Model

As was the case in Chapter 2, the received signal is defined as

$$r(t) = \Re\left\{\sum_{k=-\infty}^{\infty} S_k p(t-(\epsilon+\eta)T-kT)\alpha e^{j(2\pi f_c t+\theta)}\right\} + n(t) \qquad (-\infty < t < \infty). \tag{3.1}$$

Here, the known signal parameters are considered to be the symbol interval T, the carrier frequency f_c, and the real-valued pulse shape $p(t)$, where the pulse shape is assumed to satisfy the Nyquist ISI criterion and to be normalized to have unit energy.

The unknown signal parameters are considered to be the modulation dependent data symbols, the noise power, the fading parameters α and θ, and the time delay parameters η and ϵ. Again, S_k represents the k-th unknown modulation dependent data symbol, taken from the set of complex constellation values that define the modulation scheme used. The term $N_0/2$, where N_0 is unknown, represents the two-sided power spectral density of the white Gaussian noise process $n(t)$. The unknown fading parameters α and θ, due to the assumption of a slowly varying flat-fading channel, are considered to be constant during the observation interval. The unknown time delay is again

represented by the two unknown parameters η and ϵ, which respectively represent the integer and fractional number of symbol intervals delayed. Therefore, the total time delay is given by $(\epsilon+\eta)T$, with $0 \leq \epsilon < 1$.

3.3.1 SNR Definition

Fig. 2.1 presents the general synchronous matched filter receiver for signals of the form (3.1). In Appendix A, given the optimal sampling instant t_{opt} for the pulse shape $p(t)$, the optimal output of this receiver structure was shown to be

$$r_{n,\epsilon} = \frac{1}{2} S_{n-\eta} \alpha e^{j\theta} + noise_n, \tag{3.2}$$

where $noise_n$ is a zero mean Gaussian random variable with variance $N_0/2$. From (3.2), the average output SNR is found to be

$$SNR = \rho = \frac{E\left[|\frac{1}{2} S_{n-\eta} \alpha e^{j\theta}|^2\right]}{E\left[|noise_n|^2\right]} = \frac{\alpha^2}{2N_0}, \tag{3.3}$$

where it is assumed that the received signal utilizes a modulation scheme with a signal constellation that has been normalized to unit average energy ($E[|S_{n-\eta}|^2] = 1$).

3.4 General Formulation of the MoM-based SNR Estimator

In Chapter 2, a novel MoM-based estimator was developed for estimating α and ϵ through the use of the three moment equations

$$M_{\lambda_{i=\{1,2,3\}}} = E[|r_{n,\lambda_{i=\{1,2,3\}}}|^2] = \frac{\alpha^2}{4} \psi_{\lambda_{i=\{1,2,3\}}} + \frac{N_0}{2}, \tag{3.4}$$

where

$$\psi_{\lambda_i} = \sum_{k=-\infty}^{\infty} R(t_{n,\lambda_i})^2 = \sum_{m=-\infty}^{\infty} \left\{ \int_{-\infty}^{\infty} p(\tau) p(mT + (\lambda_i - \epsilon)T - \tau) d\tau \right\}^2. \tag{3.5}$$

In (3.4), r_{n,λ_i}, defined by (2.10), represents the output of a receiver of the form in Fig. 2.1 with a sampling instant of $t_{n,\lambda_i} = (n + \lambda_i)T$. The term λ_i is an arbitrarily chosen value with range $0 \leq \lambda_i < 1$ ($\lambda_1 \neq \lambda_2 \neq \lambda_3$), with no relationship between λ_i and the unknown time delay parameters η and ϵ assumed.

For the SNR estimator to be developed in the following, this same set of moment equations is used. Through algebraic manipulation, (3.4) can be rewritten as

$$\frac{2}{N_0} = \rho \frac{\psi_{\lambda_i}}{M_{\lambda_i}} + \frac{1}{M_{\lambda_i}}, \tag{3.6}$$

where ρ is the average output SNR defined by (3.3). As can be seen, (3.6) is a function of the unknowns N_0, ρ, and ϵ (ϵ being found in ψ_{λ_i}), while not being a function of n, η, or θ. Taking two of the three available moment equations (choosing the M_{λ_1} and M_{λ_2} equations without loss of generality), both equations can be rewritten as (3.6) and set equivalent, due to the left hand side of each equation being a function of the same unknown term $\frac{2}{N_0}$. Therefore,

$$\rho = \frac{M_{\lambda_2} - M_{\lambda_1}}{M_{\lambda_1}\psi_{\lambda_2} - M_{\lambda_2}\psi_{\lambda_1}}, \tag{3.7}$$

which can be seen to be a function of the unknowns ρ and ϵ, while the dependence on the unknown N_0 has been removed.

To further remove the dependence on one of the two remaining unknowns, the M_{λ_3} equation can be utilized. With this idea in mind, the M_{λ_3} equation is used with either of the other two moment equations (choosing the M_{λ_1} equation without loss of generality), to determine an equivalent equation for ρ through (3.7). Therefore, two ρ equations are now available, one a function of M_{λ_1} and M_{λ_2}, and the other a function of M_{λ_1} and M_{λ_3}. Setting these ρ equations equivalent and performing some algebraic manipulation[1],

$$\rho = \frac{M_{\lambda_2} - M_{\lambda_1}}{M_{\lambda_1}\psi_{\lambda_2} - M_{\lambda_2}\psi_{\lambda_1}} = \frac{M_{\lambda_3} - M_{\lambda_1}}{M_{\lambda_1}\psi_{\lambda_3} - M_{\lambda_3}\psi_{\lambda_1}}$$

$$\left(M_{\lambda_2} - M_{\lambda_1}\right)\psi_{\lambda_3} + \left(M_{\lambda_1} - M_{\lambda_3}\right)\psi_{\lambda_2} + \left(M_{\lambda_3} - M_{\lambda_2}\right)\psi_{\lambda_1} = 0. \tag{3.8}$$

Note that (3.8) is a function of only the moments M_{λ_1}, M_{λ_2}, M_{λ_3}, and the unknown fractional time delay ϵ. Therefore, analogous to the α and ϵ estimator developed in Chapter 2, if these moments can be determined, possible estimates of the unknown fractional time delay can be found by finding the zero crossings of (3.8). These estimates in turn can then be used to determine the possible ρ estimates through (3.7). Again, it is important to note that, in practice, the moments M_{λ_i} are not known *a priori* and thus must be estimated. As discussed in detail in Section 2.5.1, it was shown

[1]It should be noted that (3.8) is found no matter which two of the possible three ρ equations are set equivalent.

that these moments can be estimated through the use of a sample average of the matched filter outputs, defined by (2.17).

For the pulse shapes considered in this work, rectangular and square root-raised cosine, two possible ϵ estimates are found when determining the zero crossings of (3.8), as was the case with the α and ϵ estimator developed in Section 2.5. This results in two potential estimates for the unknown average output SNR ρ. However, in correct operation of this estimator, it was observed that these ϵ estimates correspond to a positive and negative valued estimate for the SNR. Since the SNR by definition must be positive, the correct estimate for the SNR and fractional time delay can thus easily be determined.

Based on the above discussion, the proposed asynchronous MoM-based SNR estimator can be summarized as follows:

1. Given the chosen values $\lambda_1, \lambda_2,$ and λ_3, estimate the moments $\hat{M}_{\lambda_1}$, $\hat{M}_{\lambda_2}$, and $\hat{M}_{\lambda_3}$ using the sample average estimator defined by (2.17).

2. Determine the zero-crossings of (3.8). The ϵ values corresponding to the zero-crossings are the fractional time delay estimates $\hat{\epsilon}$.

3. Using these $\hat{\epsilon}$ values, determine the corresponding SNR estimates, $\hat{\rho}$, through (3.7).

4. The final estimation values are determined by choosing the positive SNR estimate and its corresponding ϵ estimate.

3.5 Performance Analysis of the Proposed SNR Estimator

In this section, the performance of the proposed SNR estimator is shown for the cases in which the signal of (3.1) utilizes a rectangular pulse shape and a square root-raised cosine pulse shape. Previously, Sections 2.5.2 and 2.5.3 defined these pulse shapes, and presented a detailed derivation of the moments $M_{\lambda_i} = E[|r_{n,\lambda_i}|^2]$ given these pulse shapes. These same derivations are valid for the proposed SNR estimator.

For this analysis, the three moments $M_{\lambda_1=0}$, $M_{\lambda_2=1/3}$, and $M_{\lambda_3=2/3}$ are used. These moments are

estimated through the use of the sample average estimator defined by (2.17), using N_{est} uncorrelated, with respect to the noise, r_{n,λ_i} values ($i = 1, 2, 3$ and $n = n_i, n_i + 1, \ldots, n_i + (N_{est} - 1)$). In determining the zero-crossings of (3.8), the Bisection method of zero-finding is utilized [27]. For the received signal defined by (3.1), the symbol interval T is assumed to be 1, without loss of generality, and the fading model is assumed to be Rayleigh, with the average power of the fading parameter α assumed to be unity ($E[\alpha^2] = 1$). The roll-off factor, β, for the square root-raised cosine pulse shape is considered to be 0.75. Finally, the modulation schemes considered are BPSK, QPSK, 8-PSK, 16-QAM, and 64-QAM, all with signal constellations normalized to have unit average energy.

Figs. 3.1-3.4 present performance plots of the proposed SNR estimator for each of the pulse shapes considered. More specifically, in Figs. 3.1 and 3.2 for a rectangular pulse shape, and Figs. 3.3 and 3.4 for a square root-raised cosine pulse shape, the performance of the estimator is quantified through the use of the normalized mean square error (NMSE), defined as

$$\text{NMSE} = \frac{E[|\hat{\rho} - \rho|^2]}{\rho^2}, \tag{3.9}$$

as well as by the normalized estimator bias (NBIAS), defined as

$$\text{NBIAS} = \frac{E[\hat{\rho}] - \rho}{\rho}. \tag{3.10}$$

(It is worth mentioning here that, for the simulation parameters considered, the probability of SNR estimation failure was less than 1%, where an estimation failure is defined as no valid (positive) SNR estimate being found.) As can be seen from these figures, the performance of the estimator is approximately the same for each of the considered modulation schemes. Additionally, it can be observed that increasing N_{est} improves the overall performance of the estimator. This makes sense due to the fact that N_{est} defines the number of r_{n,λ_i} values used to estimate the moments from the sample average estimator defined by (2.17). The more r_{n,λ_i} values used by this estimator, the more reliable the moment estimates become, and by extension the more reliable the SNR estimate becomes.

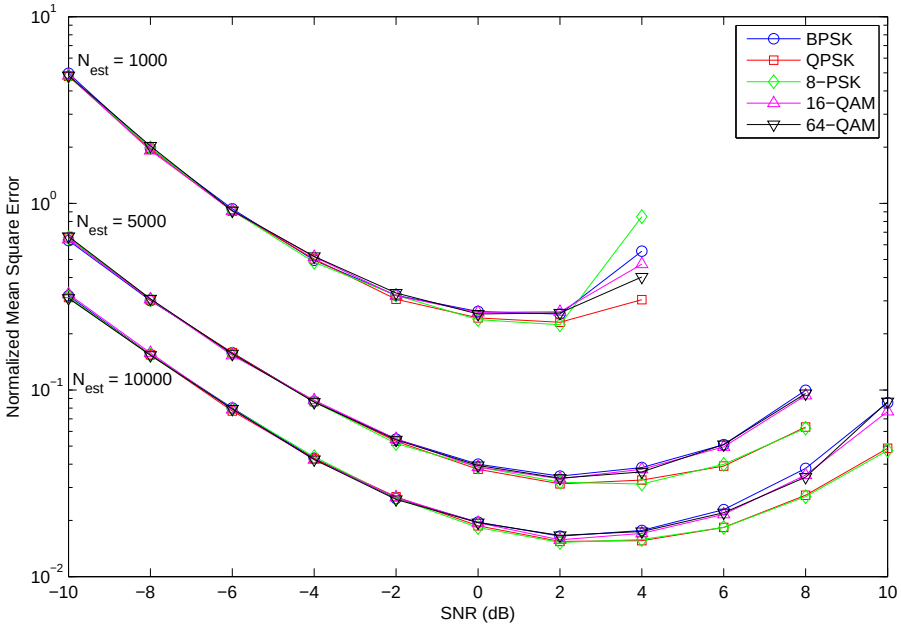

Figure 3.1: Normalized mean square error of the proposed estimator given a rectangular pulse shape.

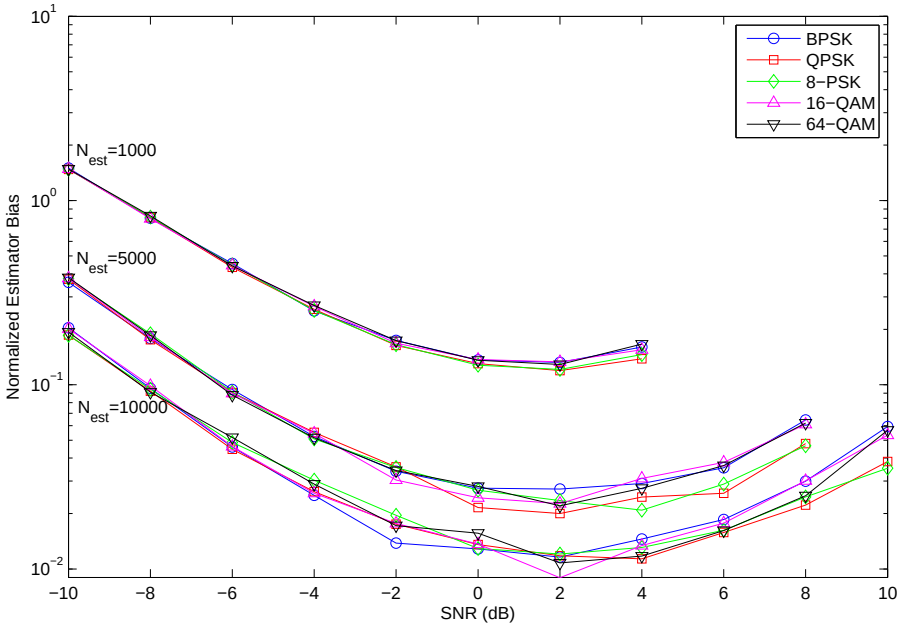

Figure 3.2: Normalized bias of the proposed estimator given a rectangular pulse shape.

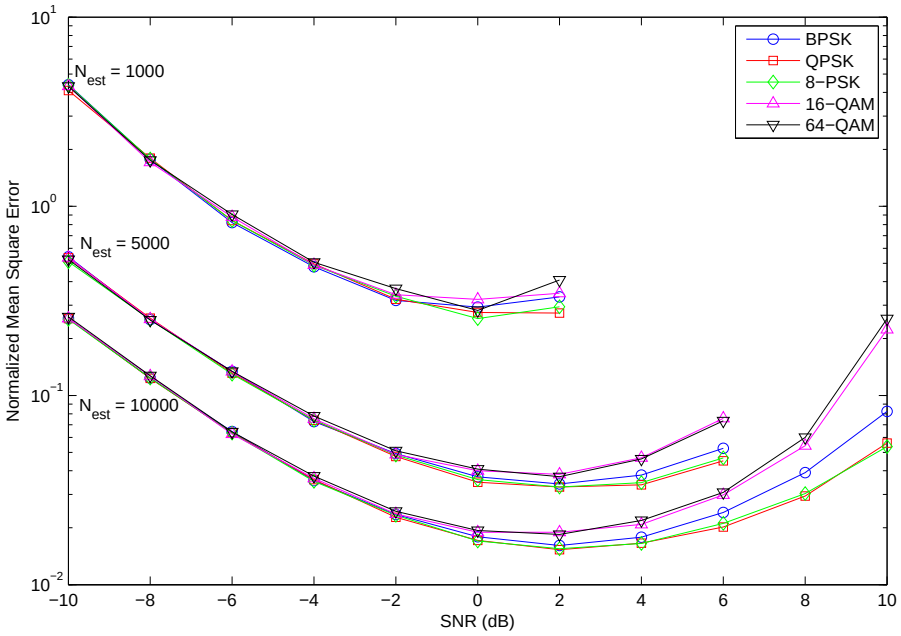

Figure 3.3: Normalized mean square error of the proposed estimator given a square root-raised cosine pulse shape ($\beta = 0.75$).

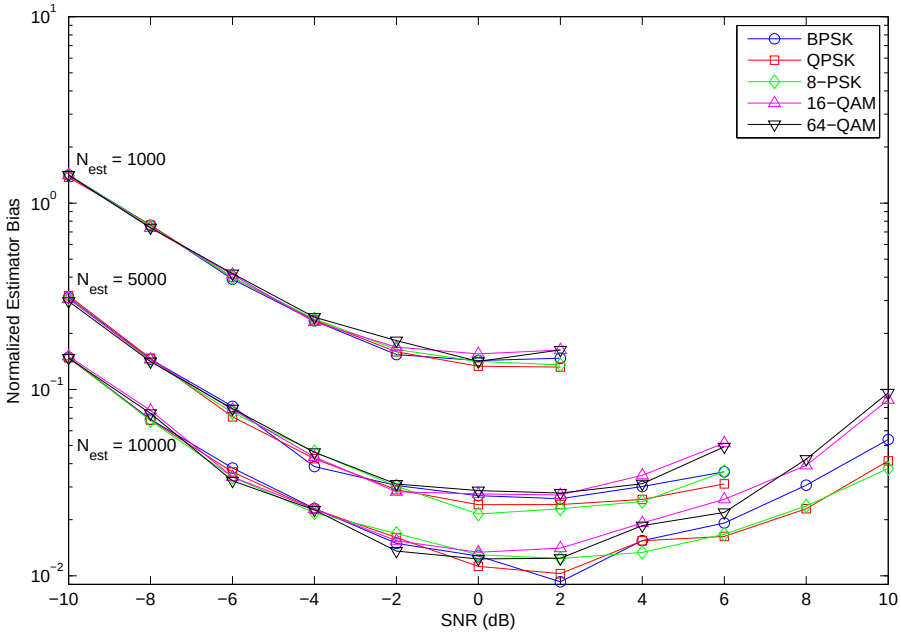

Figure 3.4: Normalized bias of the proposed estimator given a square root-raised cosine pulse shape ($\beta = 0.75$).

More interestingly, it can be observed from these figures that the NMSE and NBIAS begin to increase with increasing SNR after a certain SNR value. This effect has been observed and described for prior MoM-based, as well as non MoM-based, SNR estimation approaches, and is therefore not unique to the proposed estimator [29],[30]. As a means of better quantifying this effect, Figs. 3.5 and 3.6, for rectangular and square root-raised cosine pulse shapes respectively, present histograms for the output of the proposed SNR estimator given randomly chosen modulation schemes, excluding estimation failures, conditioned on three different true SNR values (-10dB, 0dB, and 10dB), as well as for three different values of N_{est} (1000, 5000, and 10000). From these figures, it can be observed that for true SNRs of -10dB and 10dB, the histograms have tails that are much more pronounced, and nonsymmetric, than for the histograms given a true SNR of 0dB. It is these asymmetric tails that produce the larger NMSE and NBIAS values observed at these SNRs. It is worth noting that, as expected, increasing N_{est} improves the NMSE and NBIAS by shrinking the tails of the histogram and making the tails more symmetric.

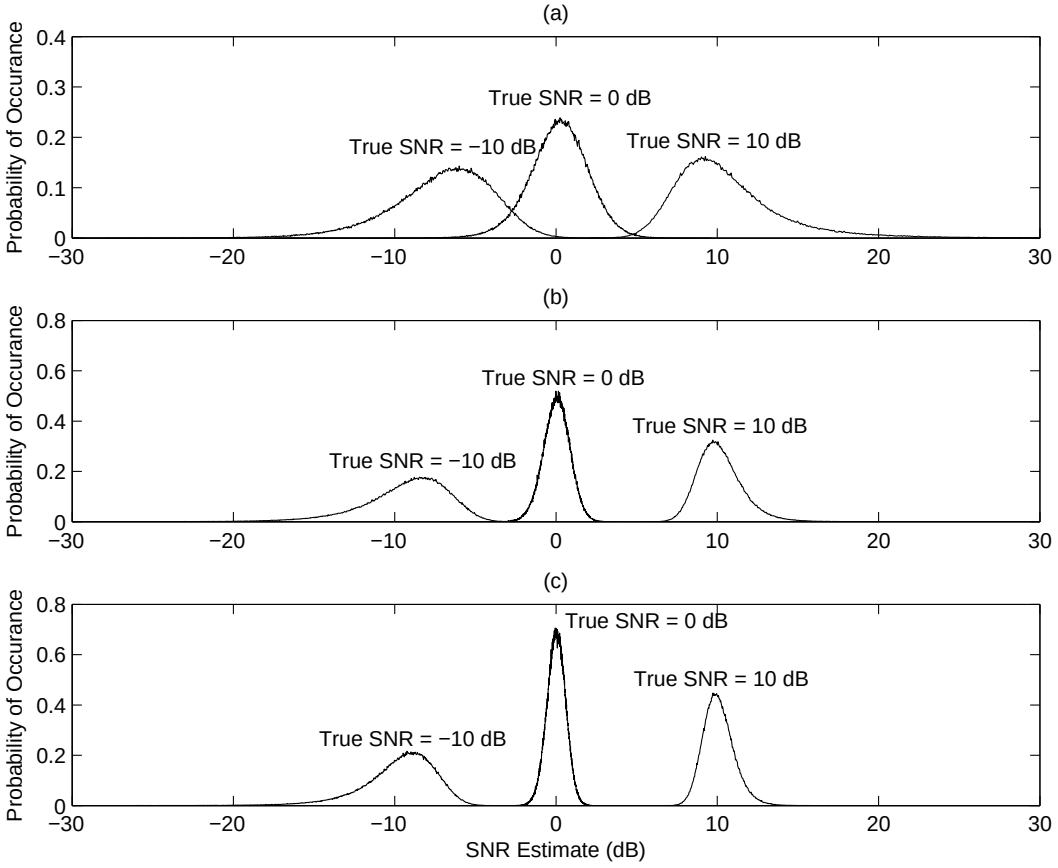

Figure 3.5: Selected histograms of the proposed estimator given a rectangular pulse shape (a. $N_{est} = 1000$, b. $N_{est} = 5000$, c. $N_{est} = 10000$)

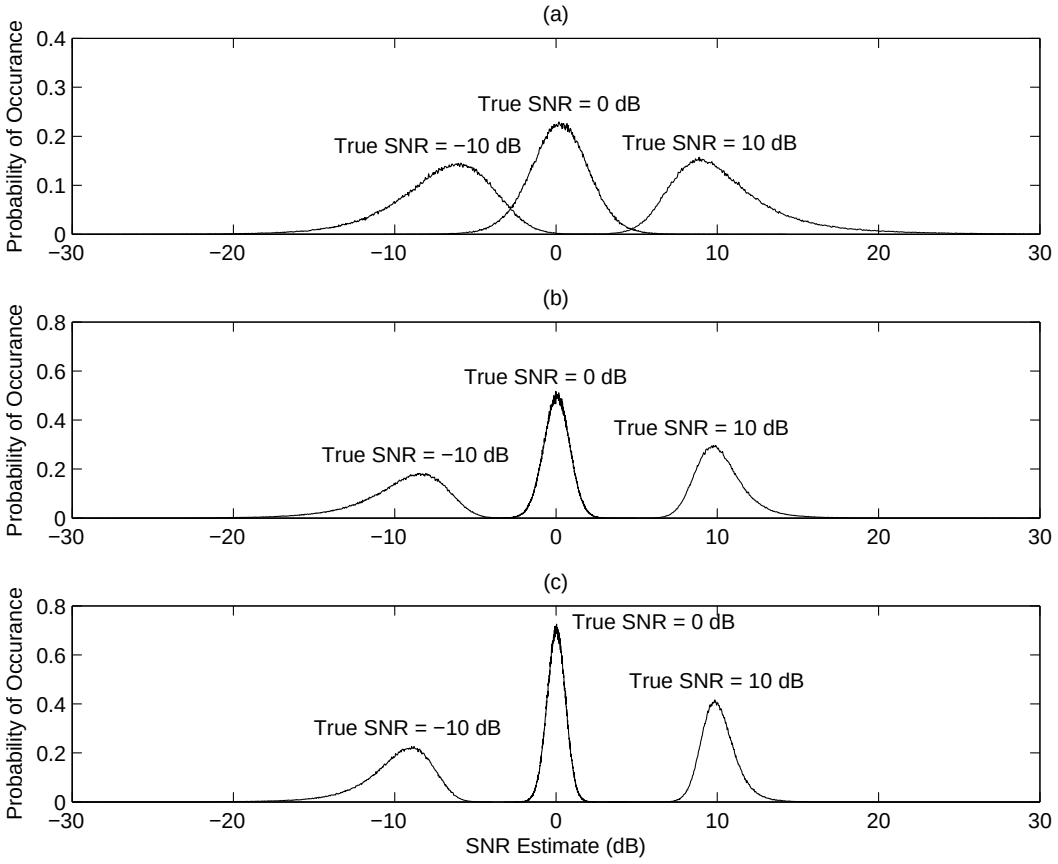

Figure 3.6: Selected histograms of the proposed estimator given a square root-raised cosine pulse shape ($\beta = 0.75$) (a. $N_{est} = 1000$, b. $N_{est} = 5000$, c. $N_{est} = 10000$)

3.6 Conclusions

In order to remove some of the more common assumptions made by prior SNR estimation techniques, this chapter proposed a novel *asynchronous*, *noncoherent*, and *non-data-aided* SNR estimator for digital amplitude-phase modulated signals in flat-fading channels. The general formulation of this estimator was presented, which applies to any pulse shape that satisfies the Nyquist ISI criterion, and is shown to utilize a method-of-moments based approach to parameter estimation similar in form to the α and ϵ estimator developed in Chapter 2.

Performance results of the proposed SNR estimator were presented considering two common pulse shapes of interest, rectangular and square root-raised cosine. More specifically, these performance results demonstrated the average normalized mean square error and average normalized bias that can be achieved by the proposed SNR estimator for a sampling of common digital amplitude-phase modulation schemes. From these results, it was observed that the performance of the proposed SNR estimator is a function of two parameters: the length of time the received signal is observed and the actual SNR of the received signal. It was shown that, in order to estimate very low, or very high, SNR values with reliability, the observation time must be adapted to compensate.

Chapter 4

Distributed Cyclic Spectrum Feature-based Modulation Classification

4.1 Motivation for Work

In single-radio spectrum sensing applications, such detrimental effects as fading and shadowing can greatly decrease the radio's ability to accurately perform spectrum sensing. Furthermore, for weak primary user signals, a single-radio system may require a very long, and perhaps impractical, sensing interval to provide for a given level of spectrum estimation accuracy. Therefore, in order to reduce the sensitivity requirements of each individual spectrum sensor, and to take advantage of radio signal variability, it is only natural to perform spectrum sensing in a distributed manner. In the literature, there has been a relatively long history of research in this area in the context of the more general problem of distributed detection and estimation theory [36],[37]. More recently, a number of papers have proposed, and partially addressed, distributed spectrum sensing in the context of cognitive radios. See [38]-[40], among others.

4.2 Contribution

In this chapter, a *novel* approach to spectrum sensing is developed in which a network of radios collaboratively detects the presence, as well as the modulation scheme, of a signal through the use of a combination of cyclic spectrum feature-based signal classification and an iterative algorithm for optimal data fusion. The development begins with a detailed discussion on both the radio-level and network-level aspects of the proposed system. After this discussion, a nonlinear Gauss-Seidel iterative algorithm is presented in order to determine the person-by-person optimal decision rules for this system. Performance analysis demonstrates that the proposed distributed system results in a significant increase in the probability of signal detection and correct modulation classification over single radio systems.

4.3 System Model of the Proposed Distributed System

Fig. 4.1 presents the block diagram of the proposed *distributed* signal detection and modulation classification system. From this diagram, it can be seen that the proposed system consists of two components. The first of these components is the set of N spectrum sensing radios. As their name implies, the function of each of these radios is to observe the transmitted signal (utilizing one of M possible modulation schemes), and based upon this observation, determine the local classification decision $u_n = i$ ($n = 1, 2, \ldots, N$ and $i = 1, 2, \ldots, M$). These local decisions are then transmitted by their respective radios to the second component of the proposed system, termed the fusion center. The function of the fusion center is to make the final global classification decision $u_0 = i$, based on its own observation of the transmitted signal and the set of N local classification decisions $\mathbf{u}$ ($\mathbf{u} = \{u_1, u_2, \ldots, u_N\}$).

In order to make this final global decision, as well as the local classification decisions u_n, decision rules must be determined for the fusion center and each radio's DM stage, respectively. In this work, "person-by-person" optimal decision rules are determined through the use of a non-linear Gauss-Seidel iterative algorithm [20]. This algorithm, and its use in determining these decision rules, is discussed in Section 4.5.

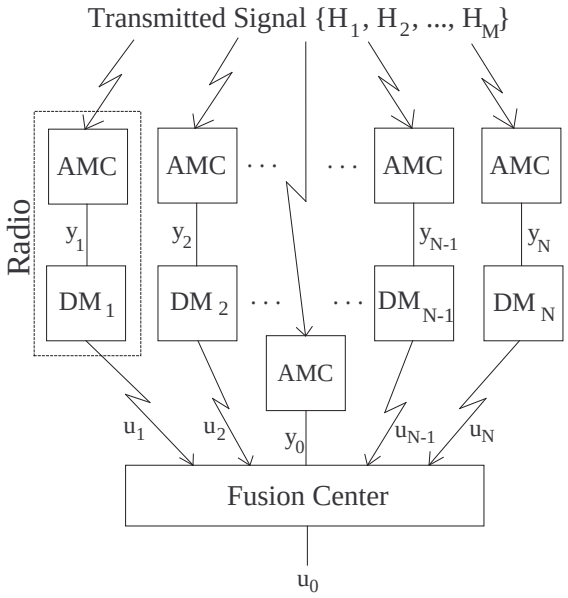

Figure 4.1: Block diagram of the proposed distributed signal detection and modulation classification system.

4.4 The Radio-Level AMC Stage

Now that the general model of the proposed distributed signal detection and modulation classification system has been described, the following two sections present in greater detail the proposed functionality of the individual spectrum sensing radios of the system. In the block diagram of Fig. 4.1, it can be seen that the N spectrum sensing radios are assumed to consist of two stages: an "automatic modulation classification" (AMC) stage and a "decision making" (DM) stage. In this section, a detailed discussion on the proposed AMC stage of the radios is presented, while in Section 4.5 a more detailed discussion is presented on the proposed DM stage of the radios.

Fig. 4.2 presents the block diagram of the proposed AMC stage. As can be seen, this stage can be broken down into two areas: feature extraction and pattern matching. The first step of the AMC stage is to observe the transmitted signal, and based upon this observation, estimate the signal's cyclic spectrum [41],[42]. The next step of the AMC stage is to determine the estimated cyclic spectrum's α-profile [9],[43]. These first two steps constitute the feature extraction aspect of the AMC stage and are discussed in more detail in Sections 4.4.1 and 4.4.2.

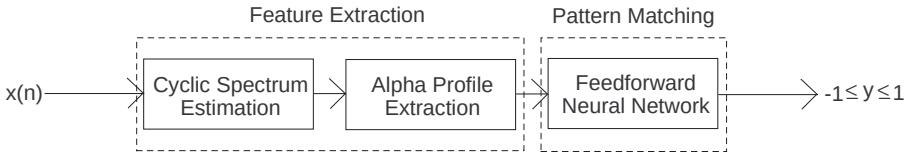

Figure 4.2: AMC stage block diagram.

In the final step of the AMC stage, the determined α-profile is used as the input to a trained feed-forward back-propagation neural network to provide the soft local classification decision y_n ($n = 1, 2, \ldots, N$). This step constitutes the pattern matching aspect of the AMC stage and is discussed in more detail in Section 4.4.3. Finally, this soft decision output is then used as the input to the radio's DM stage to determine the final local classification decision u_n. As mentioned, the decision rules used by the DM stage to determine u_n given y_n are discussed in more detail in Section 4.5.

The use of α-profiles in single radio modulation classification systems was first proposed in [9] and [43]. In these papers, α-profiles are created from the spectral coherence function, while in this work the magnitude of the cyclic spectrum is used. In regards to the use of a neural network for pattern matching, [43] utilizes a MAXNET structure with one neural network for each possible modulation scheme and a discrete output; while in this work, a single neural network and a continuous output is used. This particular setup is used in order to facilitate the determination of "person-by-person" optimal decision rules for the proposed distributed system, and is a contribution of this work.

4.4.1 Cyclic Spectrum Estimation

As mentioned, the first step of the proposed AMC stage is to estimate the cyclic spectrum, $S_x^\alpha(f)$, of the received signal [41]. In this work, this estimation is accomplished through the use of a "time-smoothing" algorithm known as the FFT Accumulation Algorithm. The purpose of this algorithm is to provide an efficient FFT-based formulation of the time-smoothed cyclic periodogram of the received signal, which can then be used to determine the cyclic spectrum estimate $\hat{S}_x^\alpha(f)$. This process is defined in more detail in the following.

From [42], the time-smoothed cyclic periodogram is defined as

$$S^{\alpha}_{x_T}(n,f)_{\Delta t} = \sum_{r} X_T(r,f_1)X^*_T(r,f_2)g(n-r), \tag{4.1}$$

where Δt is the observation time of the received signal, $f = (f_1 + f_2)/2$ is the spectral location parameter, $\alpha = f_1 - f_2$ is the spectral separation parameter, and $g(n)$ is a unity area weighting function. The terms $X_T(r, f_{\{1,2\}})$ of (4.1) are complex demodulates of the sampled received signal $x(n)$ and are defined as [42]

$$X_T(n,f) = \sum_{r=-N'/2}^{N'/2-1} a(r)x(n-r)e^{-j2\pi f(n-r)T_s}, \tag{4.2}$$

where $a(r)$ is a data tapering window (considered here to be a Hamming window) of duration $T = N'T_s$ and T_s is the sampling period. If the data tapering window $a(r)$ of (4.2) is normalized such that $\sum_r |a(r)|^2 = 1$, the time-smoothed cyclic periodogram and the cyclic spectrum have the relationship [42]

$$S^{\alpha}_x(f) = \lim_{\Delta f \to 0} \lim_{\Delta t \to \infty} S^{\alpha}_{x_T}(n,f)_{\Delta t}, \tag{4.3}$$

where $\Delta f = 1/T$. As can be seen from this relationship, given an adequate observation interval Δ_t, and appropriate data tapering window $a(r)$, the cyclic spectrum estimate $\hat{S}^{\alpha}_x(f)$ can be directly determined from the time-smoothed cyclic periodogram found through the use of the FFT Accumulation Algorithm.

4.4.2 α-Profile Determination

The next step of the spectrum sensing radio's AMC stage is to determine the α-profile from the estimated cyclic spectrum. In this work, an α-profile is determined by taking the maximum of the magnitude of the estimated cyclic spectrum along the spectral location parameter f for each value of the spectral separation parameter α. More succinctly,

$$\text{profile}(\alpha) = \max_{f} \left[\left| \hat{S}^{\alpha}_x(f) \right| \right]. \tag{4.4}$$

In the literature, α-profiles are commonly used in modulation classification systems over the complete estimate of the cyclic spectrum [9],[43]. This can be attributed to the fact that the amount of data contained in an α-profile is much smaller (by a factor of the number of samples in f) than that

contained in the cyclic spectrum estimate itself, while still providing unique, modulation specific, characteristics useful for modulation classification. This decrease in data size is useful due to the fact that it can greatly reduce the computational complexity of the pattern matching algorithm.

Figs. 4.3-4.6 present sample α-profiles (normalized to have a maximum value of 1) for BPSK, QPSK, MSK, and FSK modulated signals transmitted in an AWGN channel, under the assumption that the signals utilize a rectangular pulse shape and have an E_b/N_0 value of 10dB. These profiles are shown for only positive values of the spectral separation parameter α due to the fact that these profiles are an even function with respect to $\alpha = 0$. This characteristic of the α-profile is true for any real signal, due to the fact that the magnitude of the cyclic spectrum is itself an even function with respect to $\alpha = 0$ [41]. Therefore, when considering real signals, a further reduction in the computational complexity of the pattern matching algorithm can be achieved by removing redundancy through use of only the positive (or negative) half of the α-profiles.

4.4.3 The Feed-Forward Back-Propagation Neural Network

As previously mentioned, the proposed AMC stage can be broken down into two areas: feature extraction and pattern matching. In the previous two subsections, a discussion was presented on the steps comprising the feature extraction aspect of the AMC stage, in which a modulation dependent feature known as an α-profile is determined from observation of the transmitted signal. In this subsection, a discussion is presented on the pattern matching aspect of the AMC stage, in which an α-profile is used to determine the soft local classification decision y_n.

In this work, y_n is determined through the use of a feed-forward back-propagation neural network that has been trained using a Delta-Bar-Delta adaptive learning rate algorithm [44]. For the simulation results to be discussed in the following, the training parameters of this algorithm are:

- $\kappa = 0.035$, $\gamma = 0.333$, and $\beta = 0.7$
- An initial learning rate of 0.8.
- Four nodes in the hidden layer.
- An activation function of $\tanh(x)$ for both the hidden and output layers.

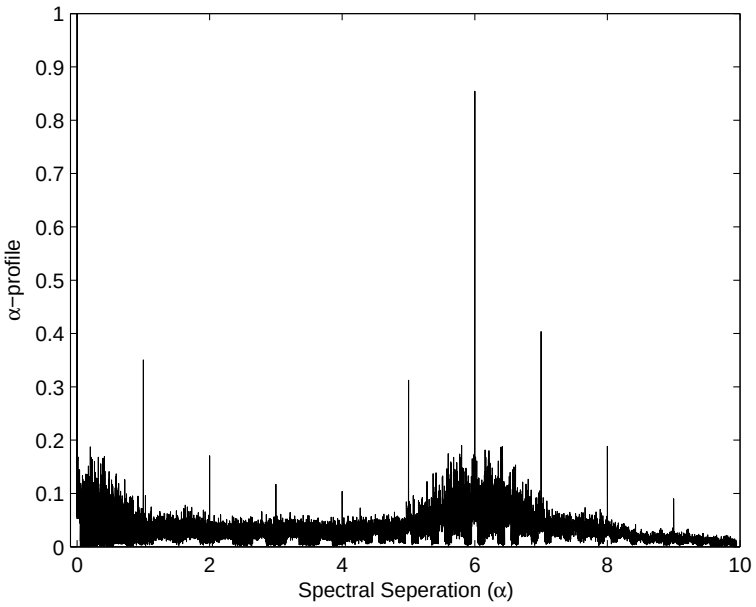

Figure 4.3: Sample α-profile for a BPSK modulated signal with an E_b/N_o of 10dB.

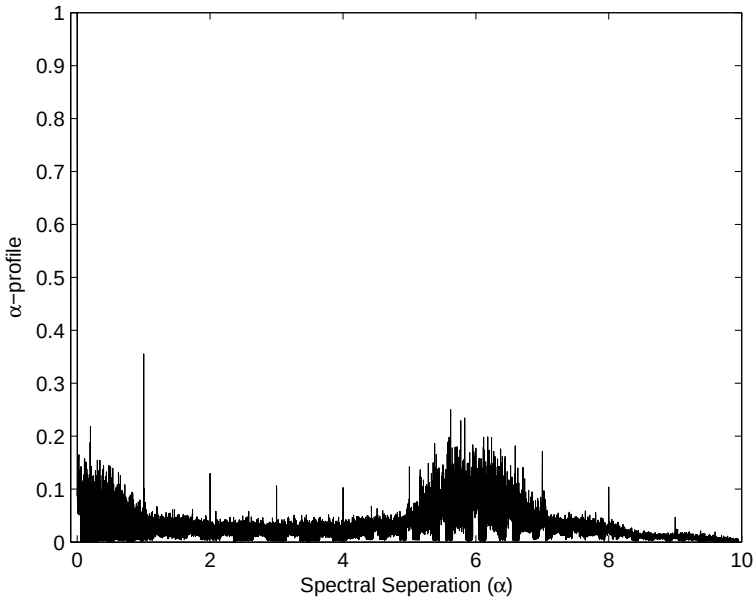

Figure 4.4: Sample α-profile for a QPSK modulated signal with an E_b/N_o of 10dB.

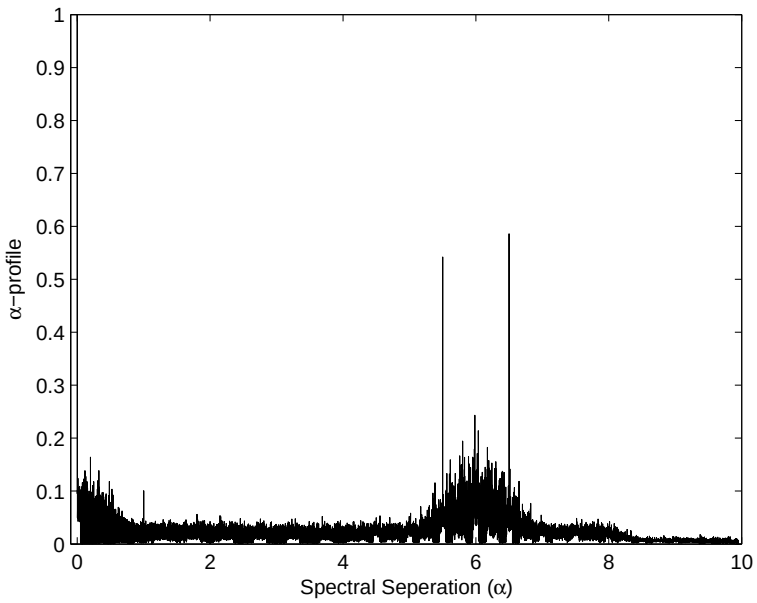

Figure 4.5: Sample α-profile for a MSK modulated signal with an E_b/N_o of 10dB.

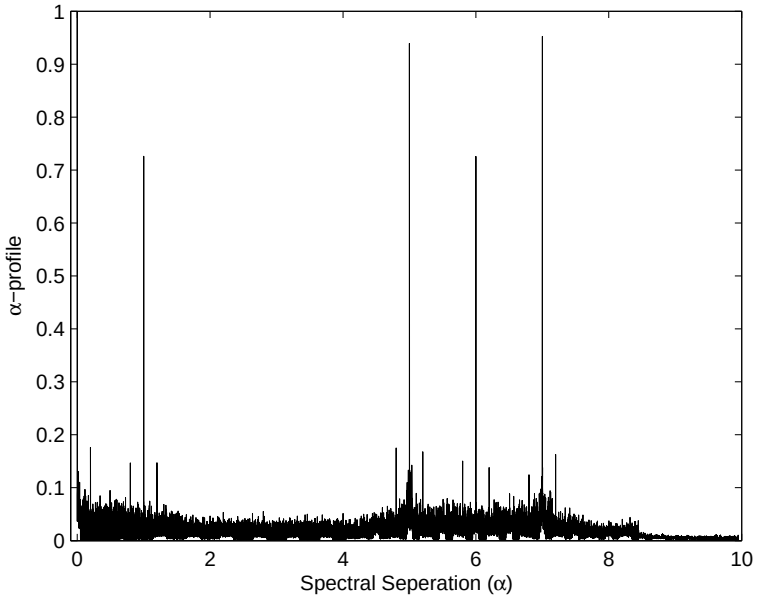

Figure 4.6: Sample α-profile for a FSK modulated signal with an E_b/N_o of 10dB.

More specifically, in this work it is considered that the training of the neural network is done off-line through the use of a set of α-profiles created from signals with known modulation schemes and E_b/N_0 values in the dB range of interest. Given this training process, the target *modulation dependent* values for the neural network output are set to be discrete values evenly spaced between -1 and 1, the range of the activation function $\tanh(x)$.

4.4.4 Simulation Results of the Proposed AMC Stage

In order to demonstrate the functionality of the proposed cyclic spectrum feature-based AMC stage, and in order to highlight the benefits of this stage on correctly detecting and classifying signals, a sample simulation is presented. For this sample simulation, it is assumed that a radio observes one of five possible signal types in an AWGN channel. The first of these signal types is assumed to be the case in which only noise is observed. The remaining four possible signal types are assumed to be a transmitted signal that utilizes a rectangular pulse shape and one of four possible modulation schemes: namely, BPSK, QPSK, MSK, or FSK. Example α-profiles for these signal types were shown previously in Figs. 4.3-4.6.

The feed-forward back-propagation neural network for this sample simulation is trained for signals with an E_b/N_0 range of -2 to 5dB through the training method described in Section 4.4.3. More specifically, a set of α-profiles were determined for each possible signal type given this E_b/N_0 range of interest and were used to train the neural network. For this training, the target *modulation dependent* values for the neural network output were defined to be: -1 for BPSK, -0.5 for FSK, 0 for noise only, 0.5 for MSK, and 1 for QPSK.

Figs. 4.7 and 4.8 present empirical conditional pdfs of the output of this trained AMC stage given signals with E_b/N_0 values of 0 and -2dB, respectively. As can be seen, the empirical conditional pdfs of the output of the trained neural network have relatively small overlap with respect to each other even at these low E_b/N_0 values. Additionally, it can be observed from these figures that the empirical conditional pdfs are concentrated around their respective target training values, as expected. For instance, the conditional pdf for the FSK signal type is concentrated around the FSK training value -0.5, while the conditional pdf for the noise only signal type is concentrated around the noise only training value 0.

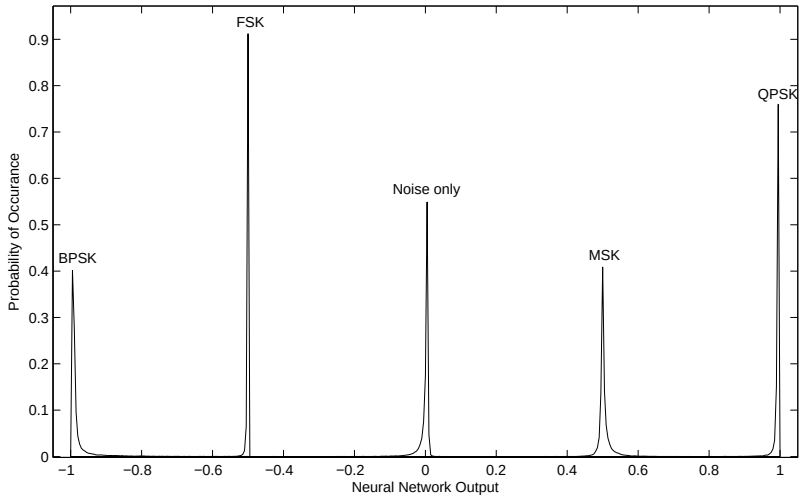

Figure 4.7: Empirical conditional probability density functions of the output of the AMC stage ($E_b/N_0 = 0$dB).

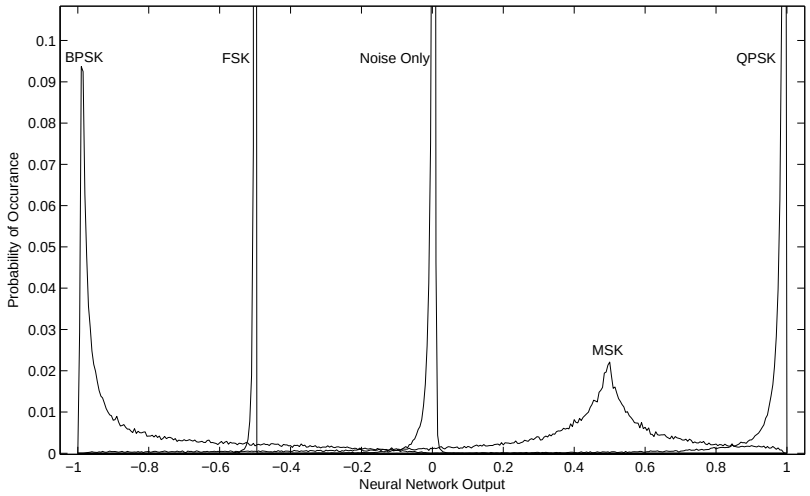

Figure 4.8: Empirical conditional probability density functions of the output of the AMC stage ($E_b/N_0 = -2$dB).

4.5 Decision Rules for the Fusion Center and the Radio-Level DM Stage

For the proposed distributed system of Fig. 4.1, it is assumed that each spectrum sensing radio's DM stage sends a local classification decision, u_n, to the fusion center in the form of a message that takes on a value in a finite alphabet (i.e. $u_n = 1, 2, \ldots, M$, where M is the number of hypotheses assumed). These u_n values are then used by the fusion center in order to determine the final global classification decision u_0. This is opposed to centralized schemes, in which each radio transmits to the fusion center its "observation" y_n. For these centralized schemes, classical detection theory still applies [24]. The distributed scheme proposed here, sharing of local decisions as opposed to observations, offers the possibility for a drastic reduction in communication requirements as opposed to a centralized scheme, at the cost of some performance reduction [36].

In the literature, there has been a relatively long history of research in distributed detection and estimation theory. For instance, person-by-person optimal decision rules for a distributed system of the form considered here, with the difference being that the fusion center does not make its own observation of the environment, were derived in [36] and [37] using a Bayesian hypothesis testing approach. For the proposed distributed system of Fig. 4.1, assuming that the local decisions made by the DMs are conditionally independent and that each radio can observe all possible hypotheses, the fusion center's person-by-person optimal decision rule has the form [20]

$$\begin{aligned} u_0 &= \arg \min_{i \in (1,\ldots,M)} \sum_{j=1}^{M} p(y_0, u_1, \ldots, u_N | H_j) P(H_j) C_{i,j} \\ &= \arg \min_{i \in (1,\ldots,M)} \sum_{j=1}^{M} p(y_0|H_j) \prod_{n=1}^{N} P(u_n|H_j) P(H_j) C_{i,j}, \end{aligned} \tag{4.5}$$

where $C_{i,j}$ is the cost of deciding $u_0 = i$ given the hypothesis H_j. Additionally, the person-by-person optimal decision rule for each radio's DM stage has the form [20]

$$u_n = \arg \min_{k \in (1,\ldots,M)} \sum_{i=1}^{M} \sum_{j=1}^{M} P(u_0 = i | u_n = k, H_j) p(y_n|H_j) P(H_j) C_{ij}. \tag{4.6}$$

It can be seen from (4.5) and (4.6) that the solution to this M-ary decentralized Bayesian hypothesis testing problem is given by a system of nonlinear equations that are coupled through the conditional

probabilities $P(u_n|H_j)$ and $P(u_0 = i|u_n = k, H_j)$. An intrinsic issue with distributed detection problems is that the computational effort required to solve these coupled decision rules becomes prohibitive as the number of spectrum sensing radios, and/or the number of hypotheses assumed, for the distributed system increases. Furthermore, Tsitsiklis and Athans show in [37] that even the simplest problems of decentralized decision making are hard from an algorithmic viewpoint, and that it becomes an NP-complete problem if the measurements at each sensor are not independent.

In order to circumvent the "brute-force" computation of these person-by-person optimal decision rules, an iterative approach based on the well-known Gauss-Seidel algorithm was proposed in [20]. This algorithm allows for a more computationally efficient means for solving the optimal decision rules, at the expense of requiring messages to be transmitted among the fusion center and the radios in the system. This algorithm consists of the following steps:

1. Choose arbitrary mappings (i.e. decision regions) for the decision rules of each radio's DM stage. From these arbitrary mappings, determine the probabilities $P(u_n|H_j)$ for all n and j.

2. Using the fusion center's decision rule, (4.5), determine the total system cost (Bayes Risk) through
$$R = \sum_{i=1}^{M} \sum_{j=1}^{M} C_{i,j} P(u_0 = i|H_j) P(H_j), \tag{4.7}$$
as well as the coupling probabilities through
$$P(u_0 = i|u_n = k, H_j) = \sum_{\mathbf{u}^n} P(u_0 = i|H_j, u_n = k, \mathbf{u}^n) \left[\prod_{q=1, q\neq n}^{N} P(u_q|H_j) \right], \tag{4.8}$$
where $\mathbf{u}^n = \{u_1, ..., u_{n-1}, u_{n+1}, ..., u_N\}$.

3. Update the mapping of the decision rule of each radio's DM stage through the use of the new coupling probabilities, (4.8), and the DMs' decision rule, (4.6).

4. Repeat Step 2, if the total cost previously found matches the new total cost (or agrees within a predefined threshold), stop. Otherwise, repeat Step 3.

4.6 Performance Analysis

In this section, two simulation cases are presented in order to demonstrate the performance gains that can be obtained when using the proposed distributed signal detection and modulation classification system over a single radio system. In each of these cases, it will be assumed that each of the radios in the distributed system are identical, and that there are 5 equally likely hypotheses ($\mathbf{H} = \{H_1, H_2, H_3, H_4, H_5\}$). For the decision rules for each of these cases, person-by-person optimal decision rules are found through the use of the Gauss-Seidel algorithm, as was defined in Section 4.5.

For the first case to be considered, the decision rules are found based upon the assumption that the output of each radio's AMC stage is a Gaussian random variable, defined as $y_n = N(m_j, \sigma)$. The mean m_j of this Gaussian random variable is defined to be dependent on the hypothesis H_j ($j = 1, 2, \ldots, 5$), while the standard deviation σ of the Gaussian random variable, considered here to be a metric of the "noise" at each radio, is not. These hypothesis dependent mean values are considered to be the following: $m_1 = 0, m_2 = -1, m_3 = 1, m_4 = -0.5$, and $m_5 = 0.5$.

Based on these assumptions, Fig. 4.9 presents the average probability of classification error for varying values of the "noise" metric σ. From this figure, it can be observed that the proposed distributed system outperforms a single radio system for all values of σ, with this gain becoming particularly more noticeable at lower values of σ. For instance, at $\sigma = 0.125$, a distributed system with 3 radios and a fusion center outperforms the single radio system by almost two orders of magnitude. Fig. 4.10 extends this analysis, for three specific values of σ, by showing the performance of the distributed system for 0 (a single radio system) to 5 radios working collaboratively with a fusion center. As can be seen from this figure, increasing the number of radios in the distributed system from 0 to 5 provides almost an order of magnitude gain in performance for these chosen σ values.

In Section 4.4.4, example empirical conditional density functions for the output of the proposed cyclic spectrum feature-based AMC stage were presented. For the second simulation case to be considered here, the decision rules are found based upon these empirical conditional density functions, as opposed to the first simulation case in which well-known conditional Gaussian distributions were

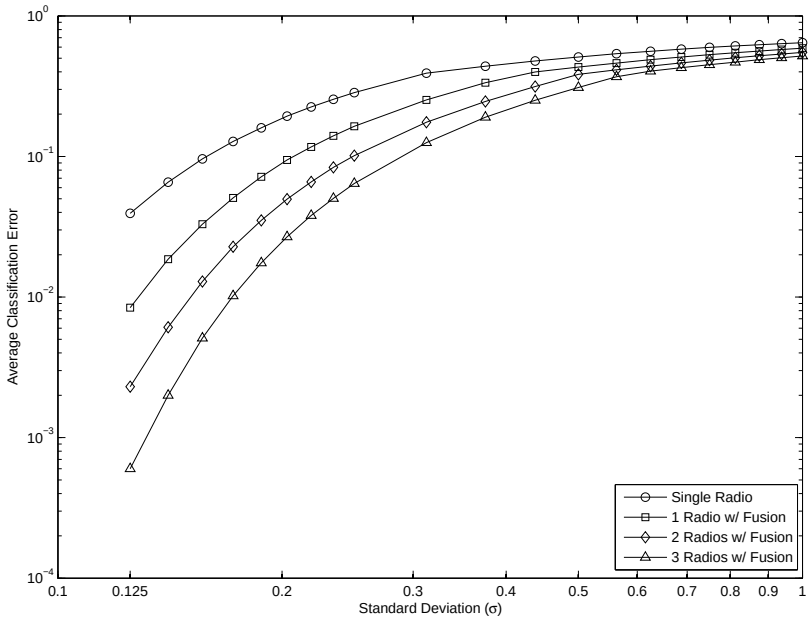

Figure 4.9: Average probability of classification error vs. σ.

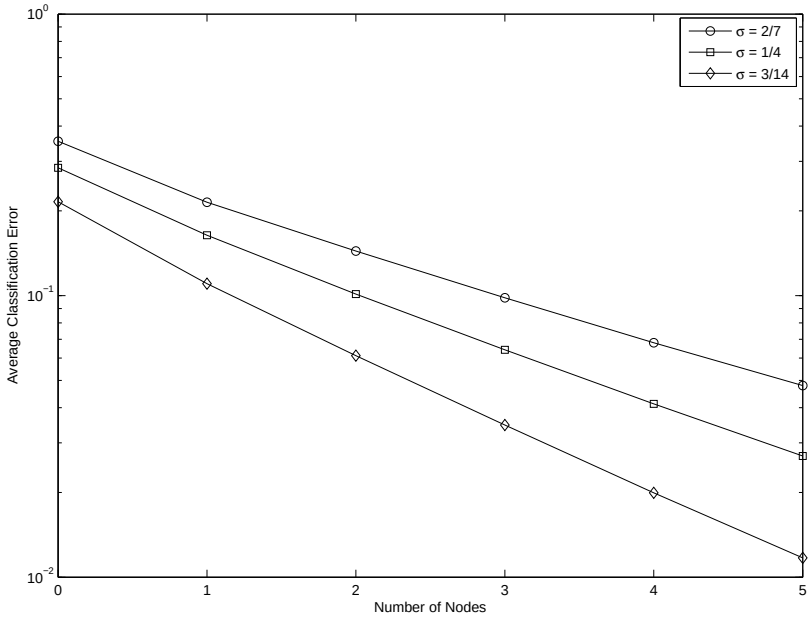

Figure 4.10: Average probability of classification error vs. number of radios.

considered. It should be noted that these empirical conditional density functions are determined based upon values of y_n that are obtained by performing two non-linear operations on the estimate of the cyclic spectrum (i.e. profiling, (4.4), and neural network-based pattern matching) . This cyclic spectrum estimate is in turn given by the multiplication of two Gaussian processes, when assuming an AWGN channel. Therefore, to the best of our knowledge, there is no closed form solution for these conditional density functions. It is for this reason that empirical conditional density functions are used.

In determining the decision rules for this simulation case (as well as for the first simulation case considered), the cost $C_{i,j}$ is given by the cost matrix

$$\mathbf{C} = \begin{pmatrix} 0 & 15 & 15 & 15 & 15 \\ 5 & 0 & 10 & 10 & 10 \\ 5 & 10 & 0 & 10 & 10 \\ 5 & 10 & 10 & 0 & 10 \\ 5 & 10 & 10 & 10 & 0 \end{pmatrix},$$

where again $C_{i,j}$ is the cost of choosing hypothesis H_i given hypothesis H_j. With respect to this second simulation case, $i = 1, 2, \ldots, 5$ and $j = 1, 2, \ldots, 5$ represent the noise only, BPSK, QPSK, FSK, and MSK hypotheses, respectively. The values of this cost matrix were chosen in order to not only penalize misclassification, but to penalize missed detection more greatly than misclassification. In other words, the highest cost value, 15, is associated with the costs $C_{0,j}$, where $j \neq 0$.

Tables 4.1-4.3 present performance results under these simulation assumptions using the empirical conditional density functions shown in Fig. 4.8 for an E_b/N_o value of -2dB. As expected, it can be seen from these tables that utilizing the proposed distributed system provides a significant performance gain over a single radio system. For example, the probability of correctly classifying MSK increases from 86.28% for a single radio system to 99.70% for a distributed system with 3 radios and a fusion center. This performance gain can be seen even more directly through observation of the average probability of classification error. This error decreases from approximately 5.16% for a single radio system to approximately 0.21% for a distributed system with 3 radios and a fusion center.

Table 4.1: Probability Matrix for the Single Radio Case

	Hypothesis				
	Noise	BPSK	QPSK	FSK	MSK
Noise	0.9721	0.0020	0.0003	0.0000	0.0150
BPSK	0.0062	0.9780	0.0015	0.0067	0.0780
QPSK	0.0000	0.0000	0.9357	0.0000	0.0420
FSK	0.0001	0.0103	0.0001	0.9933	0.0022
MSK	0.0216	0.0097	0.0624	0.0000	0.8628

Table 4.2: Probability Matrix for the Distributed Case (1 Radio with Fusion Center)

	Hypothesis				
	Noise	BPSK	QPSK	FSK	MSK
Noise	0.9953	0.0002	0.0000	0.0000	0.0016
BPSK	0.0009	0.9980	0.0000	0.0019	0.0097
QPSK	0.0000	0.0000	0.9748	0.0000	0.0184
FSK	0.0000	0.0011	0.0000	0.9981	0.0001
MSK	0.0038	0.0007	0.0252	0.0000	0.9702

Table 4.3: Probability Matrix for the Distributed Case (3 Radios with Fusion Center)

	Hypothesis				
	Noise	BPSK	QPSK	FSK	MSK
Noise	0.9985	0.0000	0.0000	0.0000	0.0000
BPSK	0.0001	0.9998	0.0000	0.0008	0.0003
QPSK	0.0000	0.0000	0.9949	0.0000	0.0027
FSK	0.0000	0.0000	0.0000	0.9992	0.0000
MSK	0.0014	0.0002	0.0051	0.0000	0.9970

4.7 Conclusions

In this chapter, a novel approach to spectrum sensing was developed based upon the *distributed* processing of local decisions made by multiple spectrum sensing radios. Performance analysis demonstrates that the proposed system provides a significant increase in the probability of signal detection and correct modulation classification over single radio systems, at the expense of requiring messages to be transmitted among the fusion center and the radios in the system. The results presented here demonstrate that, in the context of cognitive radio systems for example, performing spectrum sensing in a distributed manner can greatly increase the probability of detection (there is a radio using this frequency at this location) and correct classification (and this signal is from a primary user of the spectrum) which would ultimately lead to a lower probability of interference among systems, enabling cognitive radio systems to achieve a more efficient utilization of the spectrum.

4.8 Acknowledgement

I would like to thank Jesse D. Reed for his invaluable contributions to the ideas presented in this chapter. I especially appreciate his help on the development of the neural network and neural network training aspects used in this work, in which he played a significant role.

Chapter 5

Summary and Conclusions

Spectrum sensing is a very important function for any radio that has no, or limited, knowledge of signals in its spectral and spacial environment. It is due to this fact that spectrum sensing is a critical component in many military applications, in which enemy signals are inherently uncooperative. Additionally, spectrum sensing is a critical component in the realization of newly proposed spectrum sharing paradigms between primary licensed users and secondary cognitive radio users. It is due to these important applications that the work presented in this thesis focuses on the furthering of research in this critical area through three spectrum sensing research thrusts.

The first spectrum sensing research thrust of this thesis was described in Chapter 2. In this chapter, a novel *asynchronous* and *noncoherent* likelihood-based modulation classification system was proposed for classifying PSK/QAM modulated signals in flat-fading channels. This proposed classification system differs from prior work in classifying these signal types through the consideration of not only the fading parameters (channel gain and phase) as unknown non-data signal parameters, but also the time delay as an unknown non-data signal parameter.

The developed classifier is based upon a composite hypothesis testing approach known as the quasi-Hybrid Likelihood Ratio test. In this approach, the classifier's dependency on the unknown modulated data symbols is "averaged out" through the use of the total probability theorem, while the unknown non-data signal parameters are estimated and used by the classifier. In order to estimate the unknown channel gain and fractional time delay for use in the proposed classifier, Chapter

2 also presented a novel method-of-moments based estimation approach for these unknowns that requires no prior knowledge of the modulation scheme of the received signal. In order to quantify the performance of the proposed estimation and classification methods, simulated performance results were presented given the received signal's use of either a rectangular or square root-raised cosine pulse shape. It was shown from this analysis that the performance of the proposed estimator and classifier were a direct function of the received signal's pulse shape and signal-to-noise ratio, as well as the observation time of the signal. Finally, it was shown that the proposed classification system performs well compared to previously developed synchronous classification systems given adequate observation time.

The second spectrum sensing research thrust of this thesis was presented in Chapter 3. In this chapter, a novel *asynchronous*, *noncoherent*, and *non-data-aided* signal-to-noise ratio estimator was proposed for PSK/QAM modulated signals in flat-fading channels, in which no prior knowledge of the modulation scheme of the signal is required. This estimation approach differs from prior work in signal-to-noise ratio estimation of these signal types through the consideration of time delay as an unknown parameter. The proposed estimator was shown to be based upon an extension of the method-of-moments based estimation approach developed in Chapter 2, where here the added assumption is that the noise power of the received signal is also unknown. Simulated performance results were presented for the proposed estimator that show that the performance is a function of not only the pulse shape and observation time of the received signal, but is also a function of the true signal-to-noise ratio. More specifically, it was shown that at a certain signal-to-noise ratio, the proposed estimator's performance begins to degrade with increasing signal-to-noise ratio.

The third and final spectrum sensing research thrust of this thesis was presented in Chapter 4, in which a novel signal detection and modulation classification system was proposed based upon the *distributed* processing of local classification decisions made by multiple spectrum sensing radios. This chapter first presents the proposed functionality of the individual radios of the distributed system and can be summarized by the following steps: cyclic spectrum estimation from observation of the received signal, extraction of an α-profile from the cyclic spectrum estimate, determination of a soft decision through pattern matching of the α-profile by a trained feed-forward back-propagation neural network, and the determination of a hard decision using this soft decision and a determined

decision rule for each radio.

After the radios' functionality was described, this chapter then presented person-by-person optimal decision rules for determining the local hard decisions at each radio, as well as for determining the final global hard decision at the fusion center. An iterative approach based upon the well known Gauss-Seidel algorithm was presented in order to solve for these person-by-person optimal decision rules. Finally, simulated performance results of the proposed distributed signal detection and modulation classification system were presented. These results demonstrated the performance improvements, in terms of increased signal detection probability and lower probability of classification error, that can be achieved with the proposed distributed system over a single radio system.

Appendix A

Determining $p(r_{n,\epsilon}|S_{k,i}, H_i)$

The output of the synchronous conventional matched filter receiver of Fig. 2.1 is defined as

$$r_{n,\epsilon} = c_{n,\epsilon} - js_{n,\epsilon} = f(t_{opt}) - j \cdot g(t_{opt}), \tag{A.1}$$

where t_{opt} is the optimal sampling instant for the pulse shape $p(t)$ (defined to be the sampling instant at which no ISI is present). For the pulse shapes considered in this work, $t_{opt} = (n + \epsilon)T$. Solving for the values $f(t_{opt})$ and $g(t_{opt})$ (assuming an integer number of cycles in T and ignoring the double frequency components),

$$\begin{aligned}
f(t_{opt}) &= \int_{-\infty}^{\infty} r(\tau)\cos(2\pi f_c\tau)p(t_{opt}-\tau)d\tau \\
&= \int_{-\infty}^{\infty}\left[\Re\left\{\sum_{k=-\infty}^{\infty} S_k p(\tau-(\epsilon+\eta)T-kT)\alpha e^{j(2\pi f_c\tau+\theta)}\right\}+n(\tau)\right]\cos(2\pi f_c\tau)p(t_{opt}-\tau)d\tau \\
&= \frac{1}{2}\sum_{k=-\infty}^{\infty}\int_{-\infty}^{\infty}\Re\{S_k\}\,p(\tau-(\epsilon+\eta)T-kT)\alpha\cos(\theta)p(t_{opt}-\tau)d\tau \\
&\qquad -\frac{1}{2}\sum_{k=-\infty}^{\infty}\int_{-\infty}^{\infty}\Im\{S_k\}\,p(\tau-(\epsilon+\eta)T-kT)\alpha\sin(\theta)p(t_{opt}-\tau)d\tau + noise_{f(t_{opt})} \\
f(t_{opt}) &= \sum_{k=-\infty}^{\infty}\left\{\left[\frac{\alpha}{2}\Re\{S_k\}\cos(\theta)-\frac{\alpha}{2}\Im\{S_k\}\sin(\theta)\right]R(t_{opt})\right\}+noise_{f(t_{opt})}
\end{aligned} \tag{A.2}$$

and

$$\begin{aligned} g(t_{opt}) &= \int_{-\infty}^{\infty} r(\tau)\sin(2\pi f_c\tau)p(t_{opt}-\tau)d\tau \\ &= \int_{-\infty}^{\infty}\left[\Re\left\{\sum_{k=-\infty}^{\infty} S_k p(\tau-(\epsilon+\eta)T-kT)\alpha e^{j(2\pi f_c\tau+\theta)}\right\}+n(\tau)\right]\sin(2\pi f_c\tau)p(t_{opt}-\tau)d\tau \\ &= -\frac{1}{2}\sum_{k=-\infty}^{\infty}\int_{-\infty}^{\infty}\Re\{S_k\}\,p(\tau-(\epsilon+\eta)T-kT)\alpha\sin(\theta)p(t_{opt}-\tau)d\tau \\ &\quad -\frac{1}{2}\sum_{k=-\infty}^{\infty}\int_{-\infty}^{\infty}\Im\{S_k\}\,p(\tau-(\epsilon+\eta)T-kT)\alpha\cos(\theta)p(t_{opt}-\tau)d\tau + noise_{g(t_{opt})} \\ g(t_{opt}) &= \sum_{k=-\infty}^{\infty}\left\{-\left[\frac{\alpha}{2}\Re\{S_k\}\sin(\theta)+\frac{\alpha}{2}\Im\{S_k\}\cos(\theta)\right]R(t_{opt})\right\}+noise_{g(t_{opt})}, \end{aligned} \tag{A.3}$$

where

$$noise_{f(t_{opt})} = \int_{-\infty}^{\infty} n(\tau)\cos(2\pi f_c\tau)p(t_{opt}-\tau)d\tau, \tag{A.4}$$

$$noise_{g(t_{opt})} = \int_{-\infty}^{\infty} n(\tau)\sin(2\pi f_c\tau)p(t_{opt}-\tau)d\tau, \tag{A.5}$$

and

$$R(t_{opt}) = \int_{-\infty}^{\infty} p(\tau-(\epsilon+\eta)T-kT)p(t_{opt}-\tau)d\tau. \tag{A.6}$$

Substituting these values into (A.1), we have

$$r_{n,\epsilon} = \frac{1}{2}\alpha e^{j\theta}\sum_{k=-\infty}^{\infty}\{S_k R(t_{opt})\} + noise_n, \tag{A.7}$$

where $noise_n = noise_{f(t_{opt})} - j{\cdot}noise_{g(t_{opt})}$. Remembering that the pulse shape $p(t)$ is assumed to satisfy the Nyquist ISI criterion and to be normalized to have unit energy,

$$R(t_{opt}) = \begin{cases} 1 & \text{where } (k=n-\eta) \\ 0 & \text{otherwise} \end{cases}. \tag{A.8}$$

Therefore, given (A.8), the matched filter output can be simplified to the final form

$$r_{n,\epsilon} = \frac{1}{2}S_{n-\eta}\alpha e^{j\theta} + noise_n. \tag{A.9}$$

In (A.9), $r_{n,\epsilon}$ can be shown to be a complex Gaussian random variable conditioned on the modulated data symbol $S_{n-\eta}$ (recall that α and θ are considered deterministic). Due to this fact, the random

variable $r_{n,\epsilon}$ can be completely defined in terms of its mean and variance. The mean is found to be

$$\begin{aligned} E[r_{n,\epsilon}|S_{n-\eta}] &= E\left[\left\{\frac{1}{2}S_{n-\eta}\alpha e^{j\theta} + noise_n\right\}\Big|S_{n-\eta}\right] \\ &= E\left[\left\{\frac{1}{2}S_{n-\eta}\alpha e^{j\theta}\right\}\Big|S_{n-\eta}\right] + E[noise_n] \\ E[r_{n,\epsilon}|S_{n-\eta}] &= \frac{1}{2}S_{n-\eta}\alpha e^{j\theta} \end{aligned} \tag{A.10}$$

and the variance is found to be

$$VAR[r_{n,\epsilon}|S_{n-\eta}] = E[|r_{n,\epsilon} - E[r_{n,\epsilon}]|^2|S_{n-\eta}]$$

$$\begin{aligned} &= E\left[\left\{\int_{-\infty}^{\infty} n(\tau)\cos(2\pi f_c\tau)p(t_{opt}-\tau)d\tau\right\}^2\right] \\ &\quad + E\left[\left\{\int_{-\infty}^{\infty} n(\tau)\sin(2\pi f_c\tau)p(t_{opt}-\tau)d\tau\right\}^2\right] \\ &= \int_{-\infty}^{\infty}\int_{-\infty}^{\infty} E[n(\tau_1)n(\tau_2)]\cos(2\pi f_c\tau_1)\cos(2\pi f_c\tau_2)p(t_{opt}-\tau_1)p(t_{opt}-\tau_2)d\tau_1 d\tau_2 \\ &\quad + \int_{-\infty}^{\infty}\int_{-\infty}^{\infty} E[n(\tau_1)n(\tau_2)]\sin(2\pi f_c\tau_1)\sin(2\pi f_c\tau_2)p(t_{opt}-\tau_1)p(t_{opt}-\tau_2)d\tau_1 d\tau_2 \\ &= \int_{-\infty}^{\infty}\frac{N_0}{2}\cos(2\pi f_c\tau)^2 p(t_{opt}-\tau)^2 d\tau + \int_{-\infty}^{\infty}\frac{N_0}{2}\sin(2\pi f_c\tau)^2 p(t_{opt}-\tau)^2 d\tau \\ &= \frac{N_0}{2}\int_{-\infty}^{\infty} p(t_{opt}-\tau)^2 d\tau \end{aligned}$$

$$VAR[r_{n,\epsilon}|S_{n-\eta}] = \frac{N_0}{2}. \tag{A.11}$$

Finally, given these determined values for the mean and variance of $r_{n,\epsilon}$, the conditional probability density function $p(r_{n,\epsilon}|S_{k,i}, H_i)$ is found to be [26]

$$p(r_{n,\epsilon}|S_{k,i}, H_i) = \frac{1}{\pi VAR[r_{n,\epsilon}]}e^{-\frac{1}{VAR[r_{n,\epsilon}]}|r_{n,\epsilon}-E[r_{n,\epsilon}]|^2} = \frac{2}{\pi N_0}e^{-\frac{2}{N_0}|r_{n,\epsilon}-\frac{1}{2}\alpha e^{j\theta}S_{k,i}|^2}. \tag{A.12}$$

Bibliography

[1] United States Frequency Allocation Chart. http://www.fas.org/spp/military/program/sigint/allochrt.pdf.

[2] M. A. McHenry, "NSF spectrum occupancy measurements projects summary," Shared Spectrum Company Report, Aug. 2005.

[3] D. A. Roberson, C. S. Hood, J. L. LoCicero, and J. T. MacDonald, "Spectral occupancy and interference studies in support of cognitive radio technology deployment," in *Proc. IEEE Workshop on Netw. Technol. for Software Defined Radio Networks*, September 2006, pp. 26-35.

[4] FCC Spectrum Policy Task Force, "Report of the spectrum efficiency working group, Nov. 2002. [Online]. Available: http://www.fcc.gov/sptf/reports.html.

[5] FCC 03-322, "NPRM - Facilitating Opportunities for Flexible, Efficient, and Reliable Spectrum Use Employing Cognitive Radio Technologies," FCC, Dec. 2003.

[6] J. Mitola, "Cognitive radio: model-based competence for software radios," Ph.D. dissertation, Dept. of Teleinformatics, KTH, 1999.

[7] IEEE 802.22 Working Group on Wireless Regional Area Networks. [Online]. Available: http://www.ieee802.org/22/.

[8] A. B. MacKenzie, J. H. Reed, P. Athanas, C. W. Bostian, R. M. Buehrer, L. A. da Silva, S. W. Ellingson, Y. T. Hsiao, J. M. Park, C. Patterson, S. Raman, and C. R. C. M. da Silva, "Cognitive radio and networking research at Virginia Tech," in *Proc. of the IEEE*, vol. 97, pp. 660-688, 2009.

[9] K. Kim, I. A. Akbar, K. K. Bae, J. Um, C. M. Spooner, and J. H. Reed, "Cyclostationary approaches to signal detection and classification in cognitive radio," in *Proc. IEEE Dynamic Spectrum Access Nets.*, 2007, pp. 212-215.

[10] R. Chen, J. Park, Y. T. Hou, and J. H. Reed, "Toward secure distributed spectrum sensing in cognitive radio networks," in *IEEE Commun. Mag.*, vol. 46, pp. 50-55, 2008.

[11] Z. Quan, S. Cui, H. Poor, and A. Sayed, "Collaborative wideband sensing for cognitive radios," in *IEEE Signal Processing Mag.*, vol. 25, pp. 60-73, 2008.

[12] D. Cabric, S. M. Mishra, D. Willkomm, R. Brodersen, and A. Wolisz, "A cognitive radio approach for usage of virtual unlicensed spectrum," in *IST Movile and Wireless Commun. Summit*, 2005.

[13] T. Yucek, and H. Arslan, "A survey of spectrum sensing algorithms for cognitive radio applications," in *IEEE Commun. Surveys and Tutorials*, vol. 11, pp. 116-130, 2009.

[14] E. E. Azzouz and A. K. Nandi, *Automatic Modulation Recognition of Communication Systems.* Norwell, MA: Kluwer, 1996.

[15] W. Wei and J. M. Mendel, "Maximum-likelihood classification for digital amplitude-phase modulations," *IEEE Trans. Commun.*, vol. 48, pp. 189-193, 2000.

[16] J. A. Sills, "Maximum-likelihood modulation classification for PSK/QAM," in *Proc. IEEE MILCOM*, 1999, pp. 57-61.

[17] P. Panagiotou, A. Anastasoupoulos, and A. Polydoros, "Likelihood ratio tests for modulation classification," in *Proc. IEEE MILCOM*, 2000, pp. 670-674.

[18] A. Abdi, A. Dobre, R. Choudhry, Y. Bar-Ness, and W. Su, "Modulation classification in fading channels using antenna arrays," in *Proc. IEEE MILCOM*, 2004, pp. 211-217.

[19] A. Dobre and F. Hameed, "Likelihood-based algorithms for linear digital modulation classification in fading channels," in *Proc. IEEE CCECE/CCGEI*, 2006, pp. 1347-1350.

[20] Z. B. Tang, K. R. Pattipati, and D. L. Kleinman, "A distributed M-ary hypothesis testing problem with correlated observations," in *Proc. 28th Conf. on Decision and Control*, 1989.

[21] O. A. Dobre, A. Abdi, Y. Bar-Ness, and W. Su, "A survey of automatic modulation classification techniques: Classical approaches and new developments," *IET Commun.*, vol. 1, pp. 137-156, 2007.

[22] B. F. Beidas and C. L. Weber, "Higher-order correlation-based classification of asynchronous MFSK signal," *in Proc. IEEE MILCOM*, 1996, pp. 1003-1009.

[23] B. F. Beidas and C. L. Weber, "Asynchronous classification of MFSK signals using the higher order correlation domain," *IEEE J. Select. Areas Commun.*, vol. 46, pp. 480-493, 1998.

[24] S. M. Kay, *Fundamentals of Statistical Signal Processing: Detection Theory*. Upper Saddle River, NJ: Prentice Hall, 1993.

[25] H. L. Van Trees, *Detection, Estimation, and Modulation Theory: Part 1*. New York, NY: Wiley, 2001.

[26] S. M. Kay, *Fundamentals of Statistical Signal Processing: Estimation Theory*. Upper Saddle River, NJ: Prentice Hall, 1993.

[27] E. Kreyszig, *Advanced Engineering Mathematics, Seventh Edition*. New York, NY: Wiley, 1993.

[28] U. Mengali and A. N. D'Andrea, *Synchronization Techniques for Digital Receivers*. New York, NY: Plenum Press, 1997.

[29] M. Bakkali, A. Stephenne, S. Affes, "Generalized moment-based method for SNR estimation," in *Proc. Wireless Commun. and Netw. Conf.*, 2007, pp. 2226-2230.

[30] D. R. Pauluzzi and N. C. Beaulieu, "A comparison of SNR estimation techniques for the AWGN channel," in *IEEE Trans. Commun.*, vol. 48, pp. 1681-1691, 2000.

[31] R. M. Gagliardi and C. M. Thomas, "PCM data reliability monitoring through estimation of signal-to-noise ratio," *IEEE Trans. Commun.*, vol. COM-16, pp. 479-486, 1968.

[32] P. Gao and C. Tepedelenlioglu, "SNR estimation for non-constant modulus constellations," in *Proc. Wireless Commun. and Netw. Conf.*, vol. 1, 2004, pp. 24-29.

[33] A. Das, "NDA SNR estimation: CRLBs and EM based estimators," in *Proc. TENCON 2008*, 2008, pp. 1-6.

[34] J. Mitola III and G. Q. Maquire Jr., "Cognitive radio: making software radios more personal," *IEEE Pers. Commun.*, vol. 6, pp. 13-18, 1999.

[35] S. Haykin, "Cognitive radio: brain-empowered wireless communications," in *IEEE JSAC*, vol. 23, 2005.

[36] P. K. Varshney, *Distributed Detection and Data Fusion*. Englewood Clifffs, NY: Springer, 1997.

[37] J. N. Tsitsiklis and M. Athans, "On the complexity of decentralized decision making and detection problems," *IEEE Trans. Automatic Contr.*, vol. AC-30, pp. 440-446, 1985.

[38] A. Ghasemi and E. S. Sousa, "Collaborative spectrum sensing for opportunistic access in fading environments," in *Proc. IEEE Dynamic Spectrum Access Nets.*, Baltimore, MD, 2005, pp. 131-136.

[39] D. Cabric, A. Tkachenko, and R. W. Brodersen, "Experimental study of spectrum sensing based on energy detection and network cooperation," in *Proc. ACM Intl. Workshop Technol. and Policy for Accessing Spectr.*, Boston, MA, 2006.

[40] M. Gandetto and C. Regazzoni, "Spectrum sensing: a distributed approach for cognitive radio terminals," *IEEE J. Sel. Areasa Commun.*, vol. 25, pp. 546-557, 2007.

[41] W. A. Gardner, *Statistical Spectral Analysis: A Nonprobabilistic Theory*. Englewood Cliffs, NJ: Prentice-Hall, 1987.

[42] W. A. Gardner, *Cyclostationarity in Communications and Signal Processing*. Piscataway, NJ: IEEE Press, 1994.

[43] A. Fehske, J. Gaeddert, and J. H. Reed, "A new approach to signal classification using spectral correlation and neural networks," in *Proc. IEEE Dynamic Spectrum Access Nets.*, 2005.

[44] L. Fausett, *Fundamentals of Neural Networks - Architectures, Algorithms, and Applications*. Englewood Cliffs, NJ: Prentice-Hall, 1994.